Geosci. Model Dev. Discuss., https://doi.org/10.5194/gmd-2019-62
Manuscript under review for journal Geosci. Model Dev.
Discussion started: 25 April 2019

Geoscientific Model Development Discussions

A lattice-automaton bioturbation simulator for the coupled physics, chemistry, and biology of marine sediments (eLABS v0.1)

Yoshiki Kanzaki[1], Bernard P. Boudreau[2], Sandra Kirtland Turner[1], Andy Ridgwell[1,3]

[1]Department of Earth Sciences, University of California – Riverside, Riverside, CA 92521, USA
[2]Department of Oceanography, Dalhousie University, Halifax, Nova Scotia B3H4R2, Canada
[3]School of Geographical Sciences, University of Bristol, Bristol BS8 1SS, UK

Correspondence to: Yoshiki Kanzaki (kanzakiy@ucr.edu)

Abstract. Seawater-sediment interaction is a crucial factor in the dynamics of carbon and nutrient cycling on a wide range of spatial and temporal scales. This interaction is mediated not just through geochemistry, but also via biology. Infauna vigorously mix sediment particles, enhance porewater-seawater exchange and consequently facilitate chemical reactions. In turn, the ecology and activity of benthic fauna are impacted by their environment, amplifying the sensitivity of seawater-sediment interaction to environmental change. However, numerical representation of the bioturbation of sediment has often been treated simply as an enhanced diffusion of solutes and solids. Whilst reasonably successful in representing the mixing of bulk and predominantly oxic marine sediments, the diffusional approach to bioturbation is limited by lacking an environmental sensitivity. To better capture the mechanics and effects of sediment bioturbation, we summarize and extend a published bioturbation model (acronym: LABS) that adopts a novel lattice automaton method to simulate the behaviors of infauna that drive sediment mixing. In this new model (eLABS), simulated benthic organism behavior is combined with a deterministic calculation of water flow and oxygen and organic matter concentration fields to better reflect the physicochemical evolution of sediment. The predicted burrow geometry and mixing intensity thus attain a dependence on physicochemical sedimentary conditions. Such an interplay between biology, chemistry and physics can be important to mechanistically explain empirical observations of bioturbation and to account for the impact of environmental changes. As an illustrative example, we show how higher organic rain can drive more intense sediment mixing by 'luring' benthic organisms deeper into sediments, while lower ambient dissolved oxygen restricts the oxic habitat depth and hence tends to reduce bulk mixing rates. Finally, our model, with its oxygen and food availability controls, represents a new tool to interpret the geological record of trace fossils, e.g., burrows, as well as to mechanistically explore biological engineering of early marine environments.

1 Introduction

Geosci. Model Dev. Discuss., https://doi.org/10.5194/gmd-2019-62
Manuscript under review for journal Geosci. Model Dev.
Discussion started: 25 April 2019

Pore-water-particle reactions occurring in the upper few to hundreds of cm of a sediment column (early diagenesis) and exchange with the overlying bottom waters help regulate the chemistry of the ocean and on relatively long-time scales, atmospheric CO_2 and oxygen, and climate, e.g., Hülse et al. (2017). In turn, the rates of these reactions, and diagenesis overall, is influenced by benthic marine infauna, whose activities mix solid sediments and porewater solutes and modulate the exchange with overlying seawater. The consequent physical and chemical disturbances caused by infauna can be defined as bioturbation *sensu lato*, e.g., Aller (1982). As geological records of changing environmental conditions are often assumed to represent monotonic changes with time, and ideally ones that can be sampled at high resolution to help understand rapid events and transitions, understanding of biota-induced physicochemical disturbances is indispensable for correct interpretation of past environments, e.g., Berger et al. (1977), Trauth (1998, 2013), Meysman et al. (2006a), Ridgwell (2007), Panchuk et al. (2008), Canfield and Farquhar (2009), Hull et al. (2011), Steiner et al. (2016), and Kirtland Turner et al. (2017). Numerical models of the appropriate processes involved represent invaluable tools in this effort.

The transport of particles and porewater by infauna can be local and/or non-local, e.g., deposit feedings, depending on the biological properties of organisms and sediment environments, e.g., Aller (1982), and has been described as deterministic and/or stochastic processes, in one-, two- or three-dimensions, e.g., Aller (1980), Boudreau and Imboden (1987), Trauth (1998), Shull (2001), Meysman et al. (2003, 2006b), and Reed et al. (2006). Classic models of early diagenesis, e.g., Berner (1980), Boudreau (1996, 1997), Van Cappellen and Wang (1996), and van de Velde and Meysman (2016), on the other hand, adopt relatively simple parameterizations for particle and water mixing, usually regarded mathematically as enhanced diffusion – 'biodiffusion', because they focus more on a variety of chemical reactions occurring within sediments than on precise/realistic description of bioturbation.

The parameterizations in these models are based on modern observations, e.g., Boudreau (1994, 1998), Tromp et al. (1995), and Middelburg et al. (1997); consequently, they are not necessarily valid in the past or future environments that may be dominated by different groups of organisms, e.g., Savrda and Bottjer (1989), Aller (2001), Tarhan et al. (2015), and van de Velde et al. (2018). Nor may they be valid if, for any given ecology, changing environmental conditions lead to changes in the behavior, activity, or numbers of the individuals present.

In addition to particle mixing, benthic organisms also modify the water flow geometry within the uppermost parts of sediments, which is referred to as bioirrigation (Aller, 1982). Recent modeling studies of bioirrigation include both chemical reactions and biology-induced water-exchange processes, e.g., Meysman et al. (2007) and Volkenborn et al. (2012), but then not necessarily mixing of sediment particles. These latter studies also assume static burrow geometry and cannot simulate burrow development and the associated movement and metabolism of benthic organisms.

Geosci. Model Dev. Discuss., https://doi.org/10.5194/gmd-2019-62
Manuscript under review for journal Geosci. Model Dev.
Discussion started: 25 April 2019

Here, we build on an existing model of animal behavior and particle mixing to create a model that simulates the coupled evolution of both burrow geometry and the physicochemical environment of sediments. Our model – eLABS (v0.1) – is designed to investigate the effects of biological factors on the physicochemical environment of sediments during bioturbation, or vice versa. We provide a series of model experiments to illustrate such an application. It is also hoped that our model will promote a better understanding of trace fossils in the geological record (Olson, 2018).

2 Model overview

Our bioturbation model is a direct and traceable extension of the innovative Lattice-Automaton Bioturbation Simulator (LABS) developed by Choi et al. (2002). The automaton method can suitably represent complex animal behavior with relatively simple rules, e.g., Choi et al. (2002) and also Wolf-Gladrow (2004). We refer to our version as the 'extended' LABS (eLABS) to distinguish from the original version by Choi et al. (2002), which we hereafter refer to as just LABS. We have modified the LABS FORTRAN90 code by adding deterministic calculations of oxygen and organic matter concentrations and water flow fields to improve the representation of sediment chemistry and physics. Accordingly, eLABS runs two consecutive calculations: (i) a LABS simulation to account for stochastic animal behavior and sediment displacement, and (ii) the solution of a set of deterministic equations for water flow and oxygen and organic matter concentration fields in a coupled 2D diagenetic model. For a given time step, the behavior of benthic animals is simulated first, as well as associated non-local mixing of water, sediment, oxygen and organic matter. Within the same time step, information necessary for the deterministic calculations of oxygen and organic matter concentration and water flow fields is collected. Then, the deterministic calculations of water flow and organic matter and oxygen concentration fields are conducted via the coupled diagenetic model. This simple sequence is repeated, using the oxygen and organic matter concentration fields from the previous time step as boundary conditions for the next time step simulation of organism behavior and sediment mixing. The simulation with LABS, water flow field calculation, and calculations of organic matter and oxygen concentrations are described individually in the following subsections (see Code Availability section).

2.1 Animal behavior

The various behaviors of different benthic organisms and associated impacts on sediment mixing can be simulated in LABS, and the full details of this simulation were presented by Boudreau et al. (2001) and Choi et al. (2002), but also Reed et al. (2006) and Huang et al. (2007), so they are not repeated here. We only summarize the essential elements of LABS in this paper:

Geosci. Model Dev. Discuss., https://doi.org/10.5194/gmd-2019-62
Manuscript under review for journal Geosci. Model Dev.
Discussion started: 25 April 2019

Geoscientific Model Development Discussions

1. A simulation occurs on a grid (or lattice) that consists of sediment, water and/or organism particles (Fig. 1). The model is continuous across the left and right edges of the grid (Fig. 1). Particles on the grid either move or remain still according to the rules for individual particles.
2. Connected and coordinated organism particles represent infauna (Fig. 1). Individual organisms have their own pre-defined morphological properties, such as location and sizes of their heads and bodies (Fig. 1), as well as activity and gut fullness. Organisms move and push, ingest and/or egest sediment particles they encounter, depending on rules for each organism type. Behavioral rules for organisms contain probabilities for animal actions, which are resolved via randomly generated numbers and the state of both the organism and the properties of surrounding sediment and water particles (e.g., lability of sediment particle).
3. Sediment and water particles are essentially left static unless organisms move, push, ingest or egest sediment particles or unless it is time for sediment deposition or burial. The particle distribution is calculated with respect to a reference frame anchored at the (mean) sediment surface, which propagates upwards through the water column with time when there is sedimentation, i.e., the Berner diagenetic reference frame – see Berner (1980), and conversely loses particles at the base of the model during sedimentation.
4. Solid sediment particle properties include radioactive tracer content (e.g., ^{210}Pb) or organic matter lability, while water particles have none.

A number of input parameters are required to simulate the behavior of infauna, including physical parameters to specify the sediment conditions, e.g., sedimentation rate, sediment thickness and porosity, and biological parameters to specify the characteristics of infauna, e.g., locomotion speed and size of individual animals. In our default setting (see Section 3), we employ a 12×12 cm^2 2D sediment plus water grid, in which sediment bulk porosity is 0.8. The sediment-water interface is located at 3.6 cm below the top (Fig. 1), and sedimentation rate is 1.5×10^{-2} cm yr^{-1}. The grid cell size is 0.05×0.05 cm^2 and the grid has 0.25 cm of width with which the 2D system can be converted to a 0.25×12×12 cm^3 3D system (cf., Boudreau et al., 2001; Fig. 1). A single benthic animal is present with a 0.25×0.25×1.65 cm^3 body size (5×33 grid cells; Fig. 1), 10 cm day^{-1} locomotion speed (200 grid cells day^{-1}), and 1 g sediment (g organism)$^{-1}$ day^{-1} maximum ingestion rate (72.9 particles day^{-1}). The above animal properties represent those of a deposit feeder (e.g., Lopez and Levinton, 1987). Note that for the above unit conversion of ingestion rate from real to the 2D grid system, 2.5 and 1.2 g cm^{-3} are assumed for the densities of sediment and organism particles, respectively. The time step for simulations with this animal is 5×10^{-3} days (or 7.2 minutes).

The temporal and spatial patterns of burrows simulated by LABS can change depending on the specific rules of individual organisms. For example, in the default setting for LABS, organisms prefer to move towards more labile organic matter. When we further impose a rule to effectively cap the organisms' consumption, such that organisms with greater gut

Geosci. Model Dev. Discuss., https://doi.org/10.5194/gmd-2019-62
Manuscript under review for journal Geosci. Model Dev.
Discussion started: 25 April 2019

fullness (i.e., when they are not hungry) prefer the direction in which more water particles exist (representing a path of least resistance to travel), the resulting burrow density is lower (Fig. 2).

In LABS, the organic matter associated with a sediment particle can be parameterized with discrete lability levels. These lability levels are utilized to allow discrimination between sediment particles by organisms (e.g., Lopez and Levinton, 1987). To simulate the organic matter concentration field of sediment (see Section 2.3), we modify LABS so that each sediment particle can take a value for its organic matter concentration from a continuous distribution (from 0 to 1 wt%), instead of discrete integer levels. For convenience, changes in organic matter concentration are assumed not to change the density of a sediment particle given the limited amount of organic matter in marine sediment (e.g., ≤ 1 wt% for the present study; Section 2.3). Organisms select sediment particles on the basis of organic matter concentration, assuming that the particle is more labile when it has a larger organic matter concentration (cf., Middelburg, 1989; Canfield, 1994).

Note that in LABS, a 'particle' is better thought of as a solid 0.05×0.05×0.25 cm^3 aggregate of grains, of which a proportion of these grains can be organic matter. The size of the grains comprising a solid 0.05×0.05×0.25 cm^3 particle in the model grid is not defined but assumes to pack with no porosity. Sediment porosity is hence determined by the proportion of 0.05×0.05×0.25 cm^3 sediment particles vs. 0.05×0.05×0.25 cm^3 volumes of water.

Finally, we also impose rules in eLABS based on oxygen concentration in the water particles (see Section 2.3 for the calculation of oxygen concentration). For example, movements of benthic organisms can be restricted to within depths where the oxygen concentration is above some threshold (e.g., Huettel and Webster, 2001; Vaquer-Sunyer and Duarte, 2008). As the default setting, we impose a rule that organisms prefer to move in the direction in which the oxygen concentration is highest, i.e., organisms have little tolerance of oxygen-depleted conditions and so they avoid these conditions (Nilsson and Rosenberg, 1994).

2.2 Water flow

Significant advective water flows can be caused by infauna within sediments when they move, and/or push, ingest and/or egest sediment particles. Non-local mixing of water (bio-irrigation) by infauna is already represented in LABS (see above). In eLABS, we further implement a deterministic calculation of water flow-field, which accounts for the advective flows caused by organisms. We assume that sediment particles are impermeable (see above), and the presence of animals does not block water flows they cause (Meysman et al., 2007; Volkenborn et al., 2012), i.e., we treat organism particles in the same way as water particles. Then, the system is binary with respect to fluid flow. We solve the Navier-Stokes equation by the

Geosci. Model Dev. Discuss., https://doi.org/10.5194/gmd-2019-62
Manuscript under review for journal Geosci. Model Dev.
Discussion started: 25 April 2019

marker and cell method (Harlow and Welch, 1965; Hoffmann and Chiang, 2000; Manwart et al., 2002) for a water flow-field on the eLABS grid (Meysman et al., 2005, 2006b, 2007; Volkenborn et al., 2012):

$$\frac{\partial \mathbf{u}}{\partial t} + (\mathbf{u} \cdot \nabla)\mathbf{u} = -\frac{1}{\rho}\nabla p + \nu \nabla^2 \mathbf{u} \quad (1)$$

Here, t is time (yr), $\mathbf{u}$ is the water flow velocity vector (cm yr^{-1}), p is the pressure (g cm^{-1} yr^{-2}), and ρ and ν are respectively the density and kinematic viscosity of water (1.00 g cm^{-3} and 4.79×10^5 cm^2 yr^{-1}, respectively, at 5 °C; Kestin et al., 1978). The symbols of ∇ and ∇^2 represent the vector differential and Laplace operators, respectively. We assume negligible external forces in Eq. (1). At the top and bottom layers, we impose no-vertical-flux boundary conditions (cf., Meysman et al., 2005; Volkenborn et al., 2012) and left and right boundaries are continuous (Section 2.1). Non-slip boundaries (i.e., zero velocities) are assumed at interfaces between sediment and water/organism particles. When organisms displace sediment particles, constant flows are imposed at the middle of the head or tail of the organisms, reflecting the velocities of moved particles so that momentum is conserved. Note that, given the assumptions and boundary conditions above, the flow calculation in the present study may not be appropriate for permeable sediments, e.g., Huettel and Webster (2001). Nonetheless, the relatively fast rates of flows above the seawater-sediment interface are accounted for by considering eddy diffusion (see Section 2.3). Approximate steady-state $\mathbf{u}$ is obtained by solving Eq. (1) with time steps of 0.025 seconds until change becomes insignificant with time, which usually requires less than one model second. Figure 3 illustrates an example stream function caused by a benthic organism at 325 model days after the start of an eLABS simulation with default settings (Section 3).

2.3 Oxygen and organic matter

In LABS, a water particle has no specific physicochemical properties. In eLABS, however, water particles have individual oxygen concentrations. Sediment particles are assumed to have negligible oxygen (cf., Volkenborn et al., 2012). Organism particles are treated in the same way as water particles, i.e., they have individual oxygen concentrations. The system is then binary (sediment vs. water/organism particles) with respect to oxygen concentration. The calculation of the oxygen concentration is conducted on a grid that is occupied by water/organism particles with a general advection-diffusion-reaction equation (e.g., Boudreau, 1997):

$$\frac{\partial [\mathrm{O_2}]}{\partial t} = \nabla \cdot (D \nabla [\mathrm{O_2}] - \mathbf{u}[\mathrm{O_2}]) - R \quad (2)$$

Geosci. Model Dev. Discuss., https://doi.org/10.5194/gmd-2019-62
Manuscript under review for journal Geosci. Model Dev.
Discussion started: 25 April 2019

Geoscientific Model Development Discussions

Here, $[O_2]$ is the dissolved oxygen concentration (mol L^{-1}), D is the effective diffusion coefficient (cm^2 yr^{-1}), which accounts for eddy diffusion above seawater-sediment interface, as well as molecular diffusion, and R represents the oxygen consumption rate by aerobic decomposition of organic matter and biological respiration (mol L^{-1} yr^{-1}). Note that biological oxygen sources, which may be important for sediments in nearshore areas (e.g., Jahnke, 2001), are not considered in Eq. (2).

We adopt $D = D_0 + 0.4\nu(zu^*/\nu)^3/363$ where D_0 is the molecular diffusion coefficient (3.88×10^2 cm^2 yr^{-1} at 5 °C; Schulz, 2006), z is the height above seawater-sediment interface (cm) and u^* is the shear velocity (Boudreau, 2001; Volkenborn et al., 2012) and ν is again the kinematic viscosity of water. In our default setting, we assume that $u^* = 1.0\times10^6$ cm yr^{-1} (cf., Pope et al., 2006; Volkenborn et al., 2012). The oxygen consumption term R is given by

$$R = (k_{rsp} + k_{dcy})m[O_2] \quad (3)$$

where m is the concentration of organic matter in sediment particles (wt%) and k_{rsp} and k_{dcy} (wt%$^{-1}$ yr^{-1}) are the apparent rate constants for the biological respiration and aerobic decomposition of organic matter, respectively. Note that it has been reported that the rate of organic matter oxidation can be independent of oxygen concentration (e.g., Jørgensen and Boudreau, 2001). Nonetheless, the mechanisms which explicitly explain the oxygen dependence of organic matter oxidation in sediments are not yet fully understood (cf., Hulthe et al., 1998; Dauwe et al., 2001; Archer et al., 2002; Arndt et al., 2013).

In the present study, we assume first order dependence for Eq. (3). In our default setting, $k_{dcy} = 4.54\times10^2$ wt%$^{-1}$ yr^{-1} and $k_{rsp} = 10^4\times k_{dcy}$. Note that this k_{dcy} value corresponds to a pseudo first-order decay constant of organic matter of 0.1 yr^{-1} (cf., Canfield, 1994), if $[O_2]$ is constant at 2.2×10^{-4} mol L^{-1}. At individual interfaces between sediment and water/organism particles and the bottom layer of the grid, impermeable boundary conditions are imposed. The constant oxygen concentration (2.2×10^{-4} mol L^{-1} in the default setting; Volkenborn et al., 2012) is assumed at the top layer of the grid as another boundary condition. The default initial condition for the calculation of oxygen concentration is $[O_2] = 2.2\times10^{-4}$ mol L^{-1} for every water/organism particle. The calculation is conducted by an implicit finite-difference method.

The concentration of organic matter in sediment particles that are not consumed by benthic organisms decreases with time, according to the following equation:

$$\frac{\partial m}{\partial t} = -\gamma k_{dcy} m[O_2] \quad (4)$$

Geosci. Model Dev. Discuss., https://doi.org/10.5194/gmd-2019-62
Manuscript under review for journal Geosci. Model Dev.
Discussion started: 25 April 2019

Geoscientific Model Development Discussions

Here, γ is the unit conversion factor from mol L^{-1} to wt% (= 1.2 wt% mol^{-1} L, assuming that sediment particle has 2.5 g cm^{-3} for density, negligible porosity and CH_2O for organic matter chemical formula). For a sediment particle that is consumed by benthic animals, the concentration decreases faster:

$$\frac{\partial m}{\partial t} = -\gamma(k_{\mathrm{rsp}} + k_{\mathrm{dcy}})m[\mathrm{O}_2] \quad (5)$$

Note that, although not described by Eqs. (4) and (5), organic matter is mixed by organisms and deposited and buried along with sediment particles (as in LABS — see the first paragraph of Section 2 and Section 2.1).

As an initial condition, organic matter concentrations are randomly assigned to individual sediment particles in the range of ≤ 1 wt%, with the probability of high concentration decreasing with depth in the default setting. The sediment particles deposited to the seawater-sediment interface are assumed to have 1 wt% of organic matter (e.g., Müller and Suess, 1979) as a default setting. The calculation of organic matter concentration is conducted by an explicit finite-difference method.

3 Results and discussion

Example results with eLABS are discussed in this section. First, we consider the effects of several biological, physical and chemical factors on bioturbation on a relatively short time scale (1 model year, Section 3.1). Then, we examine temporal changes in biological and sedimentary physicochemical interactions during bioturbation by extending the simulation duration to 10 model years (Section 3.2). Finally, we illustrate the utility of eLABS for theoretical prediction of bioturbation effects with simulations for an ocean with a low oxygen concentration (Section 3.3). The model parameterizations for simulations conducted are summarized in Table 1.

3.1 One-year simulations

eLABS can yield the time evolution of oxygen and organic matter concentration profiles (e.g., Fig. 4) and fluxes of oxygen from the sediment-water interface (e.g., Fig. 5), in addition to the time evolution of burrow geometry (e.g., Fig. 6) and the biodiffusion coefficient (D_b) (e.g., Fig. 7) that can be obtained through the LABS part of the calculation. We can also calculate the relative change in sediment permeability and formation factor, which is related to tortuosity (Boudreau, 1997;

Geosci. Model Dev. Discuss., https://doi.org/10.5194/gmd-2019-62
Manuscript under review for journal Geosci. Model Dev.
Discussion started: 25 April 2019

Clennell, 1997), as functions of time through the reactive transport part of our calculation; such results are useful to the investigation of feedbacks between biological, chemical and physical factors during bioturbation.

To illustrate these feedbacks between chemistry, physics, and biology, we compare results from six simulations (Table 1): (a) a simulation with the default settings, (b) a case that assumes that organisms have tolerance to oxygen-depleted conditions but otherwise default settings, (c) a case where aerobic decomposition rate for organic matter is ten times higher, with otherwise default settings (i.e., $k_{dcy} = 4.54\times10^3$ wt%$^{-1}$ yr^{-1} and $k_{rsp} = 10^3\times k_{dcy}$), (d) a case where sediment bulk porosity is lower at 0.6, with otherwise the default settings, (e) another case that assumes ten times larger shear velocity ($u^* = 1.0\times10^7$ cm yr^{-1}), with otherwise the default settings, and (f) one without deterministic water flow, with otherwise the default settings (Figs. 4–7). All six simulations were conducted for one model year (Table 1). The effects of biological, chemical and physical parameters on bioturbation on this relatively short time scale are illustrated by comparing simulations (b) through (f) with simulation (a).

Before making these comparisons, we discuss overall flux and biodiffusion coefficient results (Figs. 5 and 7). The total oxygen consumption flux is calculated as sum of oxygen consumption flux by aerobic degradation of organic matter and the infaunal respiration flux, i.e., Eq. (3). The calculated total consumption fluxes (black dotted curves, Fig. 5) are within the ranges observed in various (from deep to coastal) marine sediment settings in the preset oceans (e.g., ~10 to 10^3 μmol cm^{-2} yr^{-1}, Jahnke, 2001; Meile and Van Cappellen, 2003), suggesting that the present model is reasonable. Oxygen consumption by respiration has been reported to be a few to several tens of μmol cm^{-2} yr^{-1} in laboratory experiments, which contain 1×10^2 to 2×10^3 individuals of infauna with body size comparable to or smaller than that assumed in the present study per m^2 (Cammen, 1980; Kemp, 1987). These observations are not inconsistent with the calculated values for the respiration flux in the present study, i.e., mostly less than a hundred (with one exception of ~600) μmol cm^{-2} yr^{-1} as annual average for simulations with 3.3×10^3 m^{-2} population. Note that infaunal respiration flux is not explicitly shown in the present study (e.g., Fig. 5) but can be calculated simply as the difference between the total O_2 consumption flux and the O_2 flux by aerobic decomposition of organic matter, i.e., black dotted curves minus turquoise curves in Fig. 5. Deviations of diffusive oxygen fluxes from total oxygen consumption fluxes represent time changes of total O_2 amount in the calculation domain.

Biodiffusion coefficients (D_b) obtained in the present study (e.g., Fig. 7) are also consistent with observed values, e.g., 10^{-3} to 10^2 cm^2 yr^{-1} at around 10^{-2} cm yr^{-1} burial velocity (Boudreau, 1994). Note that we show values of biodiffusion coefficient only for simulation (a) (denoted as $D_{b,std}$ in Fig. 7a); for other non-default simulations (b–f), we show ratios of biodiffusion coefficients to those obtained in the default run ($D_b/D_{b,std}$) to facilitate comparison. Also note that the biodiffusion coefficients in the present study are obtained by calculating average values of squared displacements of individual sediment particles divided by four times the time required to make the displacements (cf., Boudreau et al., 2001).

Geosci. Model Dev. Discuss., https://doi.org/10.5194/gmd-2019-62
Manuscript under review for journal Geosci. Model Dev.
Discussion started: 25 April 2019

Furthermore, the displacements by sediment burial are not counted in the above displacement calculation and thus not reflected in the biodiffusion coefficients.

Comparison of simulations (a) and (b) (panels (a) and (b) of Figs. 4–7) illustrates one example of the effect of a biological parameter on bioturbation. Note that benthic organisms can possess an oxygen sensor because of the fatal effects of oxygen depletion on them, while it is also possible that organisms can adapt to oxygen removal and may not require one (cf., Vaquer-Sunyer and Duarte, 2008). For example, Nilsson and Rosenberg (1994) experimentally examined responses of macrobenthos (including echinoids, bivalves, ophiuroids, polychaetes and holothuroidea) to hypoxia and reported that most of the examined species responded by escaping oxygen-depleted sediments; however, some species (the polychaetes *Nephtys incisa* and *N. hombergii*) showed greater tolerance and stayed longer in hypoxic sediments than others.

In the default setting, when the organism has little tolerance to oxygen depletion, it cannot go deeper than ~4 cm into sediments (Fig. 6a) because of the limited oxygen penetration (Fig. 4a). In contrast, when the organism has tolerance to hypoxia, i.e., simulation (b), it can move into deeper sediments despite the relative oxygen depletion (Figs. 4b and 6b). The result is deeper burrows in simulation (b) compared to (a), which facilitates oxygen transport into sediments, e.g., compare 250-days results between Figs. 4a and 4b. Nevertheless, oxygen consumption fluxes by aerobic decomposition of organic matter are similar between simulations (b) and (a), i.e., 83 vs. 88 μmol O_2 cm^{-2} yr^{-1} at 1 year. The effects of biological response to O_2 depletion on these fluxes are mitigated because we assume that organic matter concentration decreases with depth and burrow geometry differs significantly between (a) and (b) only deep within the sediments. Similarly, annual average infaunal respiration does not significantly differ between simulations (a) and (b), 62 vs. 57 μmol O_2 cm^{-2} yr^{-1} (difference between total consumption and aerobic OM decomposition from each of Figs. 5a and 5b). Note that biological respiration occurs in pulses and it is meaningful only if we compare time-averaged fluxes for respiration. We thus consider the flux values at the end of simulations for organic matter decomposition, while flux averages over the entire simulation durations for infaunal respiration, in the O_2-flux comparisons that follow, as just above. In simulation (a), the calculated D_b value is smaller than that in simulation (b) at depths deeper than ~6 cm (Fig. 7b). These differences are attributed to the low organism tolerance to hypoxia in simulation (a), which restricts sediment mixing to shallow oxygen-rich sediments, as shown through burrow geometry in Figs. 4 and 6.

Comparison of simulations (c) and (a) provides insight into the effect of greater organic matter reactivity. Because of the increase in oxygen consumption by aerobic decomposition of organic matter, oxygen cannot penetrate deeper than ~3 cm in simulation (c) (Fig. 4c), which also restricts the movement of the organism because of its low tolerance to oxygen depletion (Fig. 6c). Accordingly, oxygen consumption fluxes are comparable in simulations (a) and (c) despite the order of magnitude difference in apparent rate constants, i.e., 88 vs. 151 μmol O_2 cm^{-2} yr^{-1} at 1 year for aerobic organic matter decomposition and 62 vs. 86 μmol O_2 cm^{-2} yr^{-1} as annual averages for infaunal respiration (Figs. 5a and 5c). The limited effect on oxygen

consumption fluxes is also partially attributable to the assumed decrease of organic matter concentration with depth, which mitigates the effects of different sediment geometries especially at deep depths, and to the decreases in organic matter concentration through decomposition at shallower depths. Because sediment mixing is limited to shallow parts of sediments, the biodiffusion coefficient in simulation (c) has significantly lower values than that in (a) at depths deeper than ~5 cm (Fig. 7c). However, the biodiffusion coefficient becomes unexpectedly larger at ~7 to 8 cm depths in (c) than (a) (Fig. 7c), which could be explained by fewer, but greater sediment displacements caused by stochastic animal behavior and non-local mixing through ingestion and egestion.

We can examine the potential effects of decreased porosity on bioturbation by comparing the simulation results between (a) and (d). When porosity is decreased, oxygen penetration becomes shallower (Figs. 4a and 4d) because of increased tortuosity and lowered permeability and because the number of particles, and thus organic matter, per unit volume is higher. Accordingly, high burrow density is observed only in the shallow regions in simulation (d) because of the organism's avoidance of oxygen-depleted conditions (Fig. 6d). Despite the shallower penetration of oxygen and development of fewer deep burrows, oxygen fluxes in simulation (d) are not significantly lower than simulation (a), i.e., 78 vs. 88 μmol O_2 cm^{-2} yr^{-1} at 1 year for aerobic decomposition of organic matter and 58 vs. 62 μmol O_2 cm^{-2} yr^{-1} as annual averages for infaunal respiration (Figs. 5a and 5d). Again, this can be attributed to the increased amount of organic matter per unit volume with decreased porosity. As the bioturbated zone is relatively shallow in simulation (d), the biodiffusion coefficient is significantly reduced at ~5 to 7 cm depths, compared to (a) (Fig. 7d). We also observe an increase in the biodiffusion coefficient at ~7 to 8 cm depths in simulation (d) relative to (a) (Fig. 7d), which may be explained by the stochastic animal behavior and biology-induced non-local mixing (see the paragraph just above). We further note that the extent of oxygen penetration and biodiffusion profile are similar between simulations (d) and (c) (Figs. 4c, 4d, 7c and 7d), but the total oxygen consumption flux and burrow geometry are significantly different between the two simulations (Figs. 5c, 5d, 6c and 6d).

Next, oxygen can penetrate deeper into sediments with a higher shear velocity (simulation (e)) (Figs. 4a and 4e). With increased oxygen penetration, the oxygen consumption by infaunal respiration is larger in simulation (e) than (a), i.e., 558 vs. 62 μmol O_2 cm^{-2} yr^{-1} as annual averages (Figs. 5a and 5e). In turn, oxygen consumption by aerobic organic matter decomposition is smaller in simulation (e) than (a), 60 vs. 88 μmol O_2 cm^{-2} yr^{-1} at 1 year (Figs. 5a and 5e). The lower aerobic organic matter decay in simulation (e) is attributed to significantly higher respiration, which dominantly consumes organic matter. With deeper oxygen penetration, the burrow density, as well as the biodiffusion coefficient at deep depths, is higher in simulation (e) than (a) (Fig. 7e). Note that simulations (e) and (b) are relatively similar with respect to the biodiffusion coefficient (Figs. 7b and 7e), although different in terms of oxygen profiles and fluxes and burrow development (Figs. 4b, 4e, 5b, 5e, 6b and 6e).

Geosci. Model Dev. Discuss., https://doi.org/10.5194/gmd-2019-62
Manuscript under review for journal Geosci. Model Dev.
Discussion started: 25 April 2019

When we remove the advective flow from the calculations, i.e., simulation (f), the resultant oxygen profiles, fluxes, burrow geometry and biodiffusion coefficient are generally similar to those with the default settings (panels (a) and (f) of Figs. 4–7). Accordingly, with the assumptions adopted in the present study, advective water flow has only insignificant influences on bioturbation.

3.2 Ten-year simulations

To assess the impact on bioturbation over time scales approaching those characteristic of shallow-water, high-deposition, marine environments, we provide in this subsection 4 additional simulations run for 10 model years (Figs. 8–11 and Table 1). All the simulations assume porosity of 0.6, which enables us to detect easily the effects of greater run time on the resultant burrow geometry and biodiffusion coefficient (Figs. 6 and 7). All simulations were run without the water flow calculation to reduce the computational effort.

Specifically, we conducted simulations with (a) the default settings except for lower porosity and minus water flow (see above), (b) assuming that organisms have tolerance to hypoxia, (c) 10× higher decay constant for organic matter but otherwise the same settings as in (a), and (d) 10× higher sedimentation rate (0.15 cm yr^{-1}) but otherwise the same settings as in (a) (panels (a)–(d), respectively, of Figs. 8–11; Table 1). As in Section 3.1, we compare simulations (b) through (d) with simulation (a) to show the effects of individual parameter variations on bioturbation during 10 model years. Note that the biodiffusion coefficients in simulations (b) to (d) are shown only relative to those in (a) and absolute values of biodiffusion coefficients are given only for (a) (Fig. 11).

Comparisons of simulations (b) and (c) with (a) suggest that some of the parameter influences described in Section 3.1 hold on longer time scales but others may not. With the addition of tolerance to oxygen depletion, i.e., simulation (b), the organism can penetrate deeper sediments than in (a), resulting in correspondingly deeper burrows and increased sediment mixing (Figs. 10a, 10b and 11b), but not necessarily further oxygen penetration (Figs. 8a and 8b) depending on the structure of burrows. Also, oxygen consumption by infaunal respiration in simulation (b) is smaller than that in (a), 19 vs. 42 μmol O_2 cm^{-2} yr^{-1} as 10 years averages (Figs. 9a and 9b), probably due to the longer residence time of the organism in O_2 depleted sediments.

Aerobic decomposition of organic matter decreases with time more significantly in (a) than (b), and results in lower O_2 flux, e.g., 43 vs. 51 μmol O_2 cm^{-2} yr^{-1} at 10 years (Figs. 9a and 9b). The time change in the O_2 flux via organic matter decomposition in simulation (a) is likely caused by the fact that the organism in (a) is limited to shallow depths at first and consumes organic matter close to the seawater-sediment interface. As time passes (> 1 year), the surface sediment gets

depleted in organic matter and porewater becomes oxygenated, so that the location where decomposition of organic matter dominantly occurs shifts to deeper depths; this results in smaller rates of organic matter decomposition overall, given the assumed depth-dependence of organic matter concentration (Section 2.3). In contrast, the tolerance to hypoxia allows the organism in (b) to mix sediment more homogenously (i.e., with lateral and vertical mixing of similar intensity) despite O_2 conditions, resulting in a more time-constant O_2 flux (Fig. 9b).

With higher reactivity of organic matter, i.e., simulation (c), oxygen penetration is so limited that the organism cannot dig into sediments but mostly bulldozes the uppermost sediment particles for greater than 50 days (Figs. 8c and 10c). Accordingly, burrow development is limited to shallow sediment and sediment mixing is weaker at depth (Figs. 10a, 10c and 11c) (cf., Section 3.1). However, as time elapses (> 1 yr), burrows take a structure that allows efficient oxygen penetration and biodiffusion coefficient becomes comparable to that in (a) (Fig. 11c). O_2 consumption fluxes are comparable between simulations (c) and (a), e.g., 83 vs. 43 μmol O_2 cm^{-2} yr^{-1} at 10 years for aerobic organic matter decomposition (Figs. 9a and 9c), and 44 vs. 42 μmol O_2 cm^{-2} yr^{-1} as 10 years averages for infaunal respiration (Figs. 9a and 9c), consistent with the 1-year simulations (Section 3.1).

The effect of high sedimentation rate, which is difficult to see in short-time simulations such as those in Section 3.1, can be examined by comparing simulations (d) and (a). Sediment in (d) is less oxygenated than (a) because of the higher organic matter supply to the system (Figs. 8a and 8d). Because sediment particles with 1 wt% organic matter rain 10 times more frequently (Section 2.3), O_2 consumption fluxes are higher and remain more constant for 10 years in (d) than (a), e.g., 89 vs. 43 μmol O_2 cm^{-2} yr^{-1} at 10 years for aerobic decomposition of organic matter and 55 vs. 42 μmol O_2 cm^{-2} yr^{-1} as 10 years averages of infaunal respiration (Figs. 9a and 9d). Interestingly, sediment mixing and burrow development extend deeper into sediment in simulation (d) than (a) (Figs. 10a, 10d and 11d). We attribute the mixing enhancement in (d) to the higher frequency at which sediment particles with 1 wt% organic matter rain into burrows, which lures the organism deeper into the sediment despite less oxygenated conditions. Modern observations have suggested greater mixing by infauna in sediment that receives larger organic matter rain, e.g., Berger and Killingley (1982), Boudreau (1994, 1998), Tromp et al. (1995), Trauth et al. (1997), and Archer et al. (2002). One of mechanistic explanations for this relationship can thus be given by the present model, i.e., the deposition of relatively fresh sediment particles into infaunal burrows.

3.3 Low-O_2 simulations

The utility of models is that the potential impacts on bioturbation of animal behavior under conditions that may occur or have occurred in the future/past but cannot directly be observed through experiments, can be explored. To illustrate such an application, we consider 4 additional simulations assuming a past ocean with less oxygen (e.g., Lu et al., 2018). The four

Geosci. Model Dev. Discuss., https://doi.org/10.5194/gmd-2019-62
Manuscript under review for journal Geosci. Model Dev.
Discussion started: 25 April 2019

simulations in this subsection are parameterized in the same way as those in Section 3.2, except that the oxygen concentration at the upper boundary is taken as 0.1× that in the previous simulations (i.e., 2.2×10^{-5} mol L^{-1}). The four simulations assume (a) the default settings except for porosity, water flow and oxygen concentration (see just above and Section 3.2), (b) additionally that organisms have tolerance to hypoxia, (c) 10× higher decay constant for organic matter but otherwise the same settings as in (a), and (d) 10× higher sedimentation rate (0.15 cm yr^{-1}) but otherwise the same settings as in (a) (panels (a)–(d), respectively, of Figs. 12–15; Table 1). As in Sections 3.1 and 3.2, we compare simulations (b) through (d) with simulation (a) and describe the effects of individual parameter variations on bioturbation.

Tolerance to hypoxia allows deep burrows to develop and, consequently greater sediment mixing in simulation (b), as expected from Sections 3.1 and 3.2 (Figs. 14a, 14b and 15b). Oxygen consumptions by aerobic decomposition of organic matter are similar between simulations (a) and (b), e.g., 11 vs. 10 μmol O_2 cm^{-2} yr^{-1} at 10 years (Figs. 13a and 13b), while infaunal respiration is significantly lower in simulation (b), 2 vs. 5 μmol O_2 cm^{-2} yr^{-1} as 10 years averages (Figs. 13a and 13d), consistent with the descriptions in Section 3.2. Note that distributions of normalized oxygen concentration are not significantly changed by changing the oxygen concentration at the upper boundary (Figs. 8 and 12), because of our assumed organic matter decomposition kinetics, the equation for normalized oxygen concentration remains the same despite the change in the boundary oxygen concentration (Eqs. (2) and (3)).

The effect of assuming high reactivity for organic matter, i.e., compare panels (c) with (a) of Figs. 12–15, is generally consistent with that described in Sections 3.1 and 3.2. However, oxygen penetration remains less in (c) than (a) longer and more significantly (Figs. 12a and 12c) compared to that in Section 3.2 (Figs. 8a and 8c). Accordingly, the differences in burrow geometry and sediment mixing between the two simulations (Figs. 14a, 14c and 15c) are also more pronounced compared to those in Section 3.2 (Figs. 10a, 10c and 11c). This may be attributed to the structure of burrows in (c), which does not facilitate oxygen transport as much as that in simulation (c) of Section 3.2. Oxygen consumption via aerobic decomposition of organic matter is significantly higher in (c) than (a), 31 vs. 11 μmol O_2 cm^{-2} yr^{-1} at 10 years (Figs. 13a and 13c), while respiration fluxes are relatively similar between simulations (a) and (c), 5 vs. 3 μmol O_2 cm^{-2} yr^{-1} as 10 years averages (Figs. 13a and 13c). Lower respiration contribution to oxygen consumption in simulation (c) of this subsection than that in Section 3.2 is attributed to the longer residence of the organism in less oxygenated sediment.

High sedimentation results in shallower oxygenation of sediment (Figs. 12a and 12d) and similar oxygen consumption fluxes, e.g., 12 vs. 11 μmol O_2 cm^{-2} yr^{-1} at 10 years for aerobic decomposition of organic matter and 4 vs. 5 μmol O_2 cm^{-2} yr^{-1} as 10 years averages for infaunal respiration (Figs. 13a and 13d). With the high sedimentation, burrow development and sediment mixing are deeper (Figs. 14a, 14d and 15d), consistent with the descriptions in Section 3.2. Similar results between Sections 3.2 and 3.3 suggest that the availability of food rather than oxygen dominantly determines the preferable direction

for the organism's movement under less oxygenated conditions. Accordingly, with the assumptions in simulation (d), the modern empirical relationship between biological mixing intensity and rain rate of organic matter (e.g., Berger and Killingley, 1982; Boudreau, 1994; Tromp et al., 1995; Trauth et al., 1997; Archer et al., 2002; Section 3.2) could hold in the 10× less oxygenated oceans.

4 Summary and Conclusions

Here, we present an extension to the original LABS model of animal behavior and sediment mixing to include dissolved oxygen distributions in marine sediments and their influence on the biological processes – 'eLABS'. The results from eLABS reveal the existence of complex inter-related effects of biological, chemical and physical parameters on oxygen fluxes and rates of mixing in ocean sediments. The effects of these variations are not straightforwardly reflected in the oxygen consumption fluxes, burrow development or sediment mixing. However, we note that our example simulations consider only a limited range of variability within the full parameter space. Boudreau et al. (2001) examined variations in other biological parameters, e.g., number of infauna, locomotion speed and ingestion rate of individual organisms, and found large effects using LABS. We believe that eLABS would predict similar effects on bioturbation with variations in these same biological parameters (not tested explicitly here), but eLABS extends the ability to consider impacts on oxygen concentration and burrow geometry.

The extended LABS is useful for theoretical investigations into the interplay between biological, physical and chemical factors influencing sediment bioturbation. Our goal is ultimately to provide a mechanistic explanation for empirical relationships observed in the modern ocean sediments between bioturbation and other sediment properties and processes. Such a mechanistic understanding will be particularly useful for interpreting the extent to which bioturbation has modified geological records of past environmental events. This study has shown the above goal and application are feasible with our new model.

Further development of eLABS needs to consider an ecology of organisms that can vary in population size depending on food availability and competition for that food [Kanzaki et al., in prep.]. In addition, eLABS should include anaerobic degradation of organic matter, increased flexibility and applicability of the water flow field calculations (e.g., application to water-pumping actions by infauna; Meysman et al., 2005), and increased overall calculation efficiency to enable longer run times and/or a deeper sediment column.

Code Availability

The source codes of the extended LABS (eLABS) used for the present study as well as the original LABS are available on GitHub (https://github.com/kanzakiy/LABS), tagged as 'eLABSv0.1' and 'original_LABS', respectively, under the GNU General Public License v3.0. A readme file on the web provides the instructions for executing the model and plotting the results.

Author contributions

YK designed and implemented the model. BPB provided the latest version of LABS code. YK, SKT and AR designed the simulations. All authors contributed to the writing of the paper.

Acknowledgments

This research was supported by the Heising-Simons Foundation through a grant to A Ridgwell, S. Kirtland Turner, and L. Kump.

References

Aller, R. C.: Quantifying solute distributions in the bioturbated zone of marine sediments by defining an average microenvironment, Geochim. Cosmochim. Acta, 44, 1955–1965, doi:10.1016/0016-7037(80)90195-7, 1980.

Aller, R. C.: The effects of macrobenthos on chemical properties of marine sediment and overlying water, in Animal-Sediment Relations (P. L. McCall and M. J. S. Tevesz eds.), Springer, pp. 53–102, doi:10.1007/978-1-4757-1317-6_2, 1982.

Aller, R. C.: Transport and reactions in the bioirrigated zone, in The Benthic Boundary Layer: Transport Processes and Biogeochemistry (B. P. Boudreau and B. B. Jørgensen eds.), Oxford University Press, pp. 269– 301, 2001.

Archer, D. E., Morford, J. L., and Emerson, S. R.: A model for suboxic sedimentary diagenesis suitable for automatic tuning and gridded global domains. Global Biogeochem. Cycles, 16, 1017, doi:10.1029/2000GB001288, 2002.

Arndt, S., Jørgensen, B. B., LaRowe, D. E., Middelberg, J. J., Pancost, R. D., and Regnier, P.: Quantifying the degradation of organic matter in marine sediments: A review and synthesis, Earth-Sci. Rev., 123, 53–86, doi:10.1016/j.earscirev.2013.02.008, 2013.

Berger, W. H., and Killingley, J. S.: Box cores from the equatorial Pacific: ^{14}C sedimentation rates and benthic mixing, Mar. Geol., 45, 93–125, doi:10.1016/0025-3227(82)90182-7, 1982.

Berger, W. H., Johnson, R. F., and Killingley, J. S.: 'Unmixing' of the deep-sea record and deglacial meltwater spike, Nature, 269, 661–663, doi:10.1038/269661a0, 1977.

Berner, R. A.: Early Diagenesis: A Theoretical Approach, Princeton University Press, 1980.

Boudreau, B. P.: Is burial velocity a master parameter for bioturbation? Geochim. Cosmochim. Acta, 58, 1243–1249, doi:10.1016/0016-7037(94)90378-6, 1994.

Boudreau, B. P.: A method-of-lines code for carbon and nutrient diagenesis in aquatic sediments, Comput. Geosci., 22, 479–496, doi:10.1016/0098-3004(95)00115-8, 1996.

Boudreau, B. P.: Diagenetic Models and Their Implication, Springer, doi:10.1007/978-3-642-60421-8, 1997.

Boudreau, B. P.: Mean mixed depth of sediments: The wherefore and the why, Limnol. Oceanogr., 43, 524–526, doi:10.4319/lo.1998.43.3.0524, 1998.

Boudreau, B. P.: Solute transport above the sediment-water interface, in The Benthic Boundary Layer: Transport Processes and Biogeochemistry (B. P. Boudreau and B. B. Jørgensen eds.), Oxford University Press, pp. 104–126, 2001.

Boudreau, B. P., and Imboden, D. M.: Mathematics of tracer mixing in sediments: III. The theory of nonlocal mixing within sediments, Am. J. Sci., 287, 693–719, doi:10.2475/ajs.287.7.693, 1987.

Boudreau, B. P., Choi, J., Meysman, F., and François-Carcaillet, F.: Diffusion in a lattice-automaton model of bioturbation by small deposit feeders, J. Mar. Res., 59, 749–768, doi:10.1357/002224001762674926, 2001.

Cammen, L. M.: The significance of microbial carbon in the nutrition of the deposit feeding polychaete Nereis succinea, Mar. Biol., 61, 9–20, doi:10.1007/BF00410337, 1980.

Canfield, D. E.: Factors influencing organic carbon preservation in marine sediments, Chem. Geol., 114, 315–329, doi:10.1016/0009-2541(94)90061-2, 1994.

Canfield, D. E., and Farquhar, J.: Animal evolution, bioturbation, and the sulfate concentration of the oceans, Proc. Natl. Acad. Sci. U. S. A., 106, 8123–8127, doi:10.1073/pnas.0902037106, 2009.

Choi, J., Francois-Carcaillet, F., and Boudreau, B. P.: Lattice-automaton bioturbation simulator (LABS): implementation for small deposit feeders, Comput. Geosci., 28, 213–222, doi:10.1016/S0098-3004(01)00064-4, 2002.

Clennell, M. B.: Tortuosity: a guide through the maze, in Developments in Petrophysics (M. A. Lovell and P. K. Harvey eds.), Geological Society Special Publication No. 122, pp. 299–344, doi:10.1144/GSL.SP.1997.122.01.18, 1997.

Dade, W. B., Hogg, A. J., and Boudreau, B. P.: Physics of flow above the sediment-water interface, in The Benthic Boundary Layer: Transport Processes and Biogeochemistry (B. P. Boudreau and B. B. Jørgensen eds.), Oxford University Press, pp. 4–43, 2001.

Dauwe, B., Middelburg, J. J., and Herman, M. J.: Effect of oxygen on the degradability of organic matter in subtidal and intertidal sediments of the North Sea area, Mar. Ecol. Prog. Ser., 215, 13–22, doi:10.3354/meps215013, 2001.

Harlow, F. H., and Welch, J. E.: Numerical calculation of time-dependent viscous incompressible flow of fluid with free surface, Phys. Fluids, 8, 2182–2189, doi:10.1063/1.1761178, 1965.

Hoffmann, K. A., and Chiang, S. T.: Computational Fluid Dynamics Volume I, fourth edition, Engineering Education System, 2000.

Huang, K., Boudreau, B. P., and Reed, D. C.: Simulated fiddler-crab sediment mixing, J. Mar. Res., 65, 491–522, doi:10.1357/002224007782689120, 2007.

Huettel, M., and Webster, I. T.: Porewater flow in permeable sediments, in The Benthic Boundary Layer: Transport Processes and Biogeochemistry (B. P. Boudreau and B. B. Jørgensen eds.), Oxford University Press, pp. 144–179, 2001.

Hull, P. M., Franks, P. J. S., and Norris, R. D.: Mechanisms and models of iridium anomaly shape across the Cretaceous-Paleogene boundary, Earth Planet. Sci. Lett., 301, 98–106, doi:10.1016/j.epsl.2010.10.031, 2011.

Hulthe, G., Hulth, S., and Hall, P. O. J.: Effect of oxygen on degradation rate of refractory and labile organic matter in continental margin sediments, Geochim. Cosmochim. Acta, 62, 1319–1328, doi:10.1016/S0016-7037(98)00044-1, 1998.

Hülse, D., Arndt, S., Wilson, J. D., Munhoven, G., and Ridgwell, A.: Understanding the causes and consequences of past marine carbon cycling variability through models, Earth-Sci. Rev., 171, 349–382, doi:10.1016/j.earscirev.2017.06.004, 2017.

Jahnke, R. A.: Constraining organic matter cycling with benthic fluxes, in The Benthic Boundary Layer: Transport Processes and Biogeochemistry (B. P. Boudreau and B. B. Jørgensen eds.), Oxford University Press, pp. 302–319, 2001

Jørgensen, B. B., and Boudreau, B. P.: Diagenesis and sediment-water exchange, in The Benthic Boundary Layer: Transport Processes and Biogeochemistry (B. P. Boudreau and B. B. Jørgensen eds.), Oxford University Press, pp. 211–244, 2001.

Kanzaki, Y., Boudreau, B. P., Kirtland Turner, S., and Ridgwell, A: Marine sediment bioturbation through ecological dynamics simulated by lattice automata, in preparation.

Kemp, P. F.: Potential impact on bacteria of grazing by a macrofaunal deposit-feeder, and the fate of bacterial production, Mar. Ecol. Prog. Ser., 36, 151–161, doi:10.3354/meps036151, 1987.

Kestin, J., Sokolov, M., and Wakeham, W. A.: Viscosity of liquid water in the range −8°C to 150°C, J. Phys. Chem. Ref. Data, 7, 941–948, doi:10.1063/1.555581, 1978.

Kirtland Turner, S., Hull, P. M., Kump, L. R., and Ridgwell, A.: A probabilistic assessment of the rapidity of PETM onset, Nat. Commun., 8, 353, doi:10.1038/s41467-017-00292-2, 2017.

Lopez, G. R., and Levinton, J. S.: Ecology of deposit-feeding animals in marine sediments, Q. Rev. Biol., 62, 235–260, doi:10.1086/415511, 1987.

Lu, W., Ridgwell, A., Thomas, E., Hardisty, D. S., Luo, G., Algeo, T. J., Saltzman, M. R., Gill, B. C., Shen, Y., Ling, H.-F., Edwards, C. T., Whalen, M. T., Zhou, X., Gutchess, K. M., Jin, L., Rickaby, R. E. M., Jenkyns, H. C., Lyons, T. W.,

Lenton, T. M., Kump, L. R. and Lu, Z.: Late inception of a resiliently oxygenated upper ocean, Science, 361, 174–177, doi:10.1126/science.aar5372, 2018.

Manwart, C., Aaltosalmi, U., Koponen, A., Hilfer, R., and Timonen, J.: Lattice-Boltzmann and finite-difference simulations for the permeability for three-dimensional porous media, Phys. Rev. E, 66, 016702, doi:10.1103/PhysRevE.66.016702, 2002.

Meile, C., and Van Cappellen, P.: Global estimates of enhanced solute transport in marine sediments, Limnol. Oceanogr., 48, 777–786, doi:10.4319/lo.2003.48.2.0777, 2003.

Meysman, F. J. R., Boudreau, B. P., and Middelburg, J. J.: Relations between local, nonlocal, discrete and continuous models of bioturbation, J. Mar. Res., 61, 391–410, doi:10.1357/002224003322201241, 2003.

Meysman, F. J. R., Galaktionov, O. S., and Middelburg, J. J.: Irrigation patterns in permeable sediments induced by burrow ventilation: a case study of *Arenicola marina*, Mar. Ecol. Prog. Ser., 303, 195–202, doi:10.3354/meps303195, 2005.

Meysman, F. J. R., Middelburg, J. J., and Heip, C. H. R.: Bioturbation: a fresh look at Darwin's last idea, Trends Ecol. Evol., 21, 688–695, doi:10.1016/j.tree.2006.08.002, 2006a.

Meysman, F. J. R., Galaktionov, O. S., Gribsholt, B., and Middelburg, J. J.: Bio-irrigation in permeable sediments: An assessment of model complexity, J. Mar. Res., 64, 589–627, doi:10.1357/002224006778715757, 2006b.

Meysman, F. J. R., Galaktionov, O. S., Cook, P. L. M., Janssen, F., Huettel, M., and Middelburg, J. J.: Quantifying biologically and physically induced flow and tracer dynamics in permeable sediments, Biogeosciences, 4, 627–646, doi:10.5194/bg-4-627-2007, 2007.

Middelburg, J. J.: A simple rate model for organic matter decomposition in marine sediments, Geochim. Cosmochim. Acta, 53, 1577–1581, doi:10.1016/0016-7037(89)90239-1, 1989.

Middelburg, J. J., Soetaert, K., and Herman, P. M. J.: Empirical relationships for use in global diagenetic models, Deep-Sea Res., 44, 327–344, doi:10.1016/S0967-0637(96)00101-X, 1997.

Nilsson, H. C., and Rosenberg, R.: Hypoxic response of two marine benthic communities, Mar. Ecol. Prog. Ser., 115, 209–217, doi:10.3354/meps115209, 1994.

Olson, S. L.: Earth's Oxygenation: Causes, Consequences, and Implications for Exoplanet Life Detection, PhD Dissertation, University of California, Riverside, 2018.

Panchuk, K., Ridgwell, A., and Kump, L. R.: Sedimentary response to Paleocene-Eocene Thermal Maximum carbon release: A model-data comparison. Geology, 34, 315–318, doi:10.1130/G24474A.1, 2008.

Pope, N. D., Widdows, J., and Brinsley, M. D.: Estimation of bed shear stress using the turbulent kinetic energy approach—A comparison of annular flume and field data, Cont. Shelf Res., 26, 959–970, doi:10.1016/j.csr.2006.02.010, 2006.

Reed, D. C., Huang, K., Boudreau, B. P., and Meysman, F. J. R.: Steady-state tracer dynamics in a lattice-automaton model of bioturbation, Geochim. Cosmochim. Acta, 70, 5855–5867, doi:10.1016/j.gca.2006.03.026, 2006.

Ridgwell, A.: Interpreting transient carbonate compensation depth changes by marine sediment core modeling, Paleoceanogr. Paleoclimatol., 22, PA4102, doi:10.1029/2006PA001372, 2007.

Savrda, C. E., and Bottjer, D. J.: Trace-fossil model for reconstructing oxygenation histories of ancient marine bottom waters: application to Upper Cretaceous Noibrara Formation, Colorado, Palaeogeogr. Palaeoclimatol. Palaeoecol., 74, 49–74, doi:10.1016/0031-0182(89)90019-9, 1989.

Schulz, H. D.: Quantification of early diagenesis: dissolved constituents in pore water and signals in the solid phase, in Marine Geochemistry (H. D. Schulz and M. Zabel eds.), Springer, Berlin, Heidelberg, pp. 73–124, doi: 10.1007/3-540-32144-6_3, 2006.

Shull, D. H.: Transition-matrix model of bioturbation and radionuclide diagenesis, Limnol. Oceanogr. 46, 905–916, doi:10.4319/lo.2001.46.4.0905, 2001.

Steiner, Z., Lazar, B., Levi, S., Tsroya, S., Pelled, O., Bookman, R., and Erez, J.: The effect of bioturbation in pelagic sediments: Lessons from radioactive tracers and planktonic foraminifera in the Gulf of Aqaba, Red Sea, Geochim. Cosmochim. Acta, 194, 139–152, doi:10.1016/j.gca.2016.08.037, 2016.

Tarhan, L. G., Droser, M. L., Planavsky, N. J., and Johnson, D. T.: Protracted development of bioturbation through the early Paleozoic Era, Nat. Geosci., 8, 865–869, doi:10.1038/ngeo2537, 2015.

Trauth, M. H.: TURBO: A dynamic-probabilistic simulation to study the effects of bioturbation on paleoceanographic time series, Comput. Geosci., 24, 433–441, doi:10.1016/S0098-3004(98)00019-3, 1998.

Trauth, M. H.: TURBO2: A MATLAB simulation to study the effects of bioturbation on paleoceanographic time series, Comput. Geosci., 61, 1–10, doi:10.1016/j.cageo.2013.05.003, 2013.

Trauth, M. H., Sarnthein, M., and Arnold, M.: Bioturbational mixing depth and carbon flux at the seafloor, Paleoceanography, 12, 517–526, doi:10.1029/97PA00722, 1997.

Tromp, T. K., Van Cappellen, P., and Key, R. M.: A global model for the early diagenesis of organic carbon and organic phosphorous in marine sediments, Geochim. Cosmochim. Acta, 59, 1259–1284, doi:10.1016/0016-7037(95)00042-X, 1995.

Van Cappellen, P., and Wang, Y.: Cycling of iron and manganese in surface sediments: a general theory for the coupled transport and reaction of carbon, oxygen, nitrogen, sulfur, iron, and manganese, Am. J. Sci., 296, 197–243, doi:10.2475/ajs.296.3.197, 1996.

van de Velde, S., and Meysman, F. J. R.: The influence of bioturbation on iron and Sulphur cycling in marine sediments: a model analysis, Aquat. Geochem., 22, 469–504, doi:10.1007/s10498-016-9301-7, 2016.

van de Velde, S., Mills, B. J. W., Meysman, F. J. R., Lenton, T. M., and Poulton, S. W.: Early Palaeozoic ocean anoxia and global warming driven by the evolution of shallow burrowing, Nat. Commun., 9, 2554, doi:10.1038/s41467-018-04973-4, 2018.

Vaquer-Sunyer, R., and Duarte, C. M.: Thresholds of hypoxia for marine biodiversity, Proc. Natl. Acad. Sci. U. S. A., 105, 15452–15457, doi:10.1073/pnas.0803833105, 2008.

Volkenborn, N., Meile, C., Polerecky, L., Pilditch, C. A., Norkko, A., Norkko, J., Hewitt, J. E., Thrush, S. F., Wethey, D. S., and Woodin, S. A.: Intermittent bioirrigation and oxygen dynamics in permeable sediments: An experimental and modeling study of three tellinid bivalves, J. Mar. Res., 70, 794–823, doi:10.1357/002224012806770955, 2012.

Wolf-Gladrow, D. A.: Lattice-Gas Cellular Automata and Lattice Boltzmann Models: An Introduction, Springer, doi:10.1007/b72010, 2004.

Figure captions

Figure 1. Illustration of grid on which the behavior of benthic organism is simulated by the Lattice-Automaton Bioturbation Simulator (LABS). Note that the left and right boundaries of the grid are continuous. Shown in lower right is a magnified view where each grid cell (0.05×0.05 cm^2) can be seen. Dashed lines are drawn to show the implicit width of the system with which the 2D grid system can be converted to a 3D system.

Figure 2. Geometry of burrows after 1-year simulations by LABS with different rules for the preferred direction of organism movements. In (a), the preferred direction is where more labile organic matter exists. In (b), an additional rule is imposed upon the rules in (a), that organisms with greater gut fullness prefer to move in the direction where more water exists.

Figure 3. Stream function calculated at 325 model days from the start of a simulation with eLABS using the default settings (Section 3).

Figure 4. Time evolution of oxygen profiles calculated for 1-year simulations by eLABS. Six different simulations were conducted (Section 3.1): (a) with the default settings, (b) assuming organisms to have tolerance to oxygen-depleted conditions but otherwise the default settings, (c) with 10× higher rate for aerobic decomposition of organic matter but otherwise the default settings, (d) with 0.6 of porosity but otherwise the default settings, (e) with 10× higher shear velocity but otherwise the default settings, and (f) without the deterministic water flow calculation with otherwise the default settings. Shown are the profiles of oxygen concentration normalized to the constant boundary value (2.2×10^{-4} mol L^{-1}) at the top layer of the grid at 25, 50, 100, 150, 200 and 250 model days from the start of the simulations.

Figure 5. Time evolution of oxygen fluxes obtained from 1-year simulations with eLABS. See Section 3.1 and caption of Fig. 4 for the details on simulations (a–f). Black dotted curves represent the total oxygen consumption fluxes, orange curves the fluxes of oxygen supply via molecular plus eddy diffusion, and turquoise curves the oxygen consumption fluxes through aerobic degradation of organic matter. Note that the scale of vertical axis is different in (e).

Figure 6. Time evolution of burrow geometry obtained from 1-year simulations with eLABS. See Section 3.1 and caption of Fig. 4 for the details on simulations (a–f). Shown are burrow geometries at 25, 50, 100, 150, 200 and 250 model days from the start of the simulations.

Geosci. Model Dev. Discuss., https://doi.org/10.5194/gmd-2019-62
Manuscript under review for journal Geosci. Model Dev.
Discussion started: 25 April 2019

Geoscientific Model Development Discussions

Figure 7. Time evolution of biodiffusion coefficient (D_b) obtained from 1-year simulations with eLABS. See Section 3.1 and caption of Fig. 4 for the details on simulations (a–f). Note that the D_b values are presented only for simulation (a) (denoted as $D_{b,std}$); for other simulations (b–f), the ratios of D_b values to those in (a) ($D_b/D_{b,std}$) are shown to facilitate comparison and dashed vertical lines are references to denote $D_b = D_{b,std}$. Plotted are these values/ratios at 25, 50, 75, …, 350 model days from the start of the simulations.

Figure 8. Time evolution of oxygen profiles calculated from 10-year simulations with eLABS. Four different simulations were conducted (Section 3.2): (a) with low porosity and no advective water flow, but otherwise the default settings, (b) additionally assuming organisms to have tolerance to oxygen-depleted conditions, (c) with 10× higher rate for aerobic decomposition of organic matter but otherwise the same settings as in (a), and (d) with 10× higher sedimentation rate but otherwise the same settings as in (a). Shown are the profiles of oxygen concentration normalized to the constant boundary value (2.2×10^{-4} mol L^{-1}) at the top layer of the grid at 25, 50 and 100 model days and 1, 5 and 10 model years from the start of the simulations.

Figure 9. Time evolution of oxygen fluxes obtained from 10-year simulations with eLABS. See Section 3.2 and caption of Fig. 8 for the details on simulations (a–d). Black dotted curves represent the total oxygen consumption fluxes, orange curves the fluxes of oxygen supply via molecular plus eddy diffusion, and turquoise curves the oxygen consumption fluxes through aerobic degradation of organic matter.

Figure 10. Time evolution of burrow geometry obtained from 10-year simulations with eLABS. See Section 3.2 and caption of Fig. 8 for the details on simulations (a–d). Shown are burrow geometries at 25, 50 and 100 model days and 1, 5 and 10 model years from the start of the simulations.

Figure 11. Time evolution of biodiffusion coefficient (D_b) obtained from 10-year simulations with eLABS. See Section 3.2 and caption of Fig. 8 for the details on simulations (a–d). Note that the D_b values are presented only for simulation (a) (denoted as $D_{b,std}$); for other simulations (b–d), the ratios of D_b values to those in (a) ($D_b/D_{b,std}$) are shown to facilitate comparison and dashed vertical lines are references to denote $D_b = D_{b,std}$. Plotted are these values/ratios at 25 model days to 10 model years from the start of the simulations with intervals of 25 model days.

Figure 12. Time evolution of oxygen profiles calculated from 10-year simulations with eLABS. Four different simulations were conducted (Section 3.3): (a) with low porosity, no advective water flow and 10× lower oxygen concentration for seawater, but otherwise the default settings, (b) additionally assuming organisms to have tolerance to oxygen-depleted conditions, (c) with 10× higher rate for aerobic decomposition of organic matter but otherwise the same settings as in (a), and (d) with 10× higher sedimentation rate but otherwise the same settings as in (a). Shown are the profiles of oxygen concentration normalized to the constant boundary value (2.2×10^{-5} mol L^{-1}) at the top layer of the grid at 25, 50 and 100 model days and 1, 5 and 10 model years from the start of the simulations.

Figure 13. Time evolution of oxygen fluxes obtained from 10-year simulations with eLABS. See Section 3.3 and caption of Fig. 12 for the details on simulations (a–d). Black dotted curves represent the total oxygen consumption fluxes, orange curves the fluxes of oxygen supply via molecular plus eddy diffusion, and turquoise curves the oxygen consumption fluxes through aerobic degradation of organic matter.

Figure 14. Time evolution of burrow geometry obtained from 10-year simulations with eLABS. See Section 3.3 and caption of Fig. 12 for the details on simulations (a–d). Shown are burrow geometries at 25, 50 and 100 model days and 1, 5 and 10 model years from the start of the simulations.

Geosci. Model Dev. Discuss., https://doi.org/10.5194/gmd-2019-62
Manuscript under review for journal Geosci. Model Dev.
Discussion started: 25 April 2019

Geoscientific Model Development Discussions
Open Access
EGU

Figure 15. Time evolution of biodiffusion coefficient (D_b) obtained from 10-year simulations with eLABS. See Section 3.3 and caption of Fig. 12 for the details on simulations (a–d). Note that the D_b values are presented only for simulation (a) (denoted as $D_{b,std}$); for other simulations (b–d), the ratios of D_b values to those in (a) ($D_b/D_{b,std}$) are shown to facilitate comparison and dashed vertical lines are references to denote $D_b = D_{b,std}$. Plotted are these values/ratios at 25 model days to 10 model years from the start of the simulations with intervals of 25 model days.

Geosci. Model Dev. Discuss., https://doi.org/10.5194/gmd-2019-62
Manuscript under review for journal Geosci. Model Dev.
Discussion started: 25 April 2019

Geoscientific Model Development Discussions
Open Access
EGU

Table 1. Model parameterization.

Parameter [a]	Section 3.1 (Figs. 4–7)						Section 3.2 (Figs. 8–11)				Section 3.3 (Figs. 12–15)			
	(a)	(b)	(c)	(d)	(e)	(f)	(a)	(b)	(c)	(d)	(a)	(b)	(c)	(d)
Tolerance to hypoxia [b]	F	T	F	F	F	F	F	T	F	F	F	T	F	F
OM decomposition rate (10^2 wt%$^{-1}$ yr^{-1})	4.54	4.54	45.4	4.54	4.54	4.54	4.54	4.54	45.4	4.54	4.54	4.54	45.4	4.54
Porosity	0.8	0.8	0.8	0.6	0.8	0.8	0.6	0.6	0.6	0.6	0.6	0.6	0.6	0.6
Shear velocity (10^6 cm yr^{-1})	1	1	1	1	10	1	1	1	1	1	1	1	1	1
Advective flow [b]	T	T	T	T	T	F	F	F	F	F	F	F	F	F
Sedimentation rate (10^{-2} cm yr^{-1})	1.5	1.5	1.5	1.5	1.5	1.5	1.5	1.5	1.5	15	1.5	1.5	1.5	15
Oxygen concentration (10^{-4} mol L^{-1})	2.2	2.2	2.2	2.2	2.2	2.2	2.2	2.2	2.2	2.2	0.22	0.22	0.22	0.22
Simulation duration (yr)	1	1	1	1	1	1	10	10	10	10	10	10	10	10

[a] See Sections 2 and 3 for the details.

[b] 'F' denotes that simulation either assumes no tolerance to hypoxia for organisms or does not account for advective water flow caused by animal movements. 'T' denotes the opposite parameterization to 'F'.

Geosci. Model Dev. Discuss., https://doi.org/10.5194/gmd-2019-62
Manuscript under review for journal Geosci. Model Dev.
Discussion started: 25 April 2019

Geoscientific Model Development Discussions

Figure 1

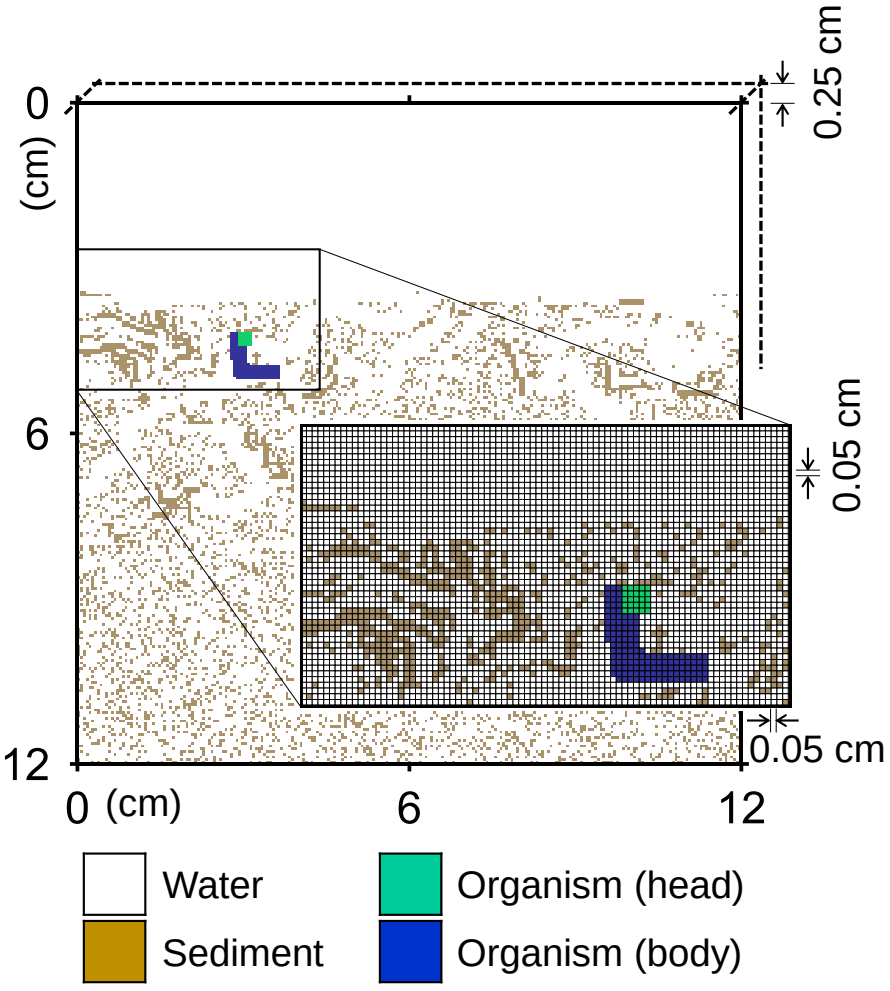

Geosci. Model Dev. Discuss., https://doi.org/10.5194/gmd-2019-62
Manuscript under review for journal Geosci. Model Dev.
Discussion started: 25 April 2019

Geoscientific Model Development Discussions
Open Access
EGU

Figure 2

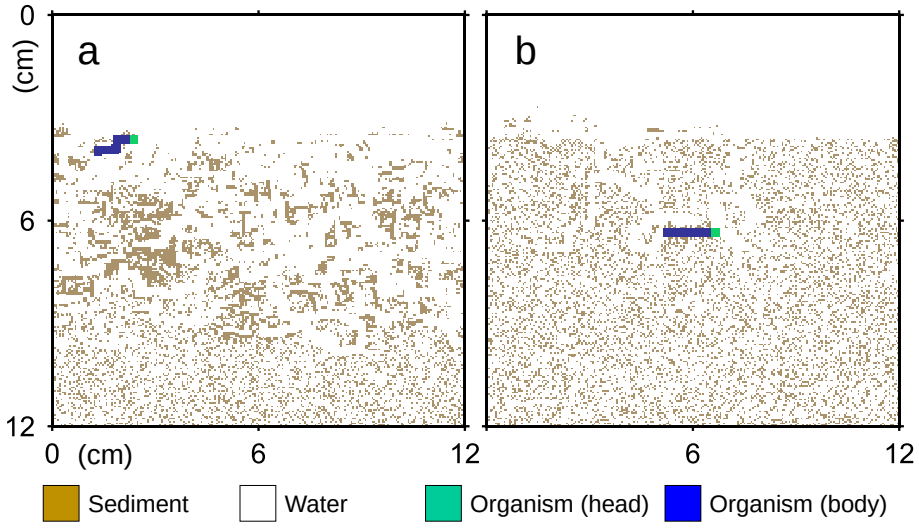

Geosci. Model Dev. Discuss., https://doi.org/10.5194/gmd-2019-62
Manuscript under review for journal Geosci. Model Dev.
Discussion started: 25 April 2019

Geoscientific Model Development Discussions
Open Access
EGU

Figure 3

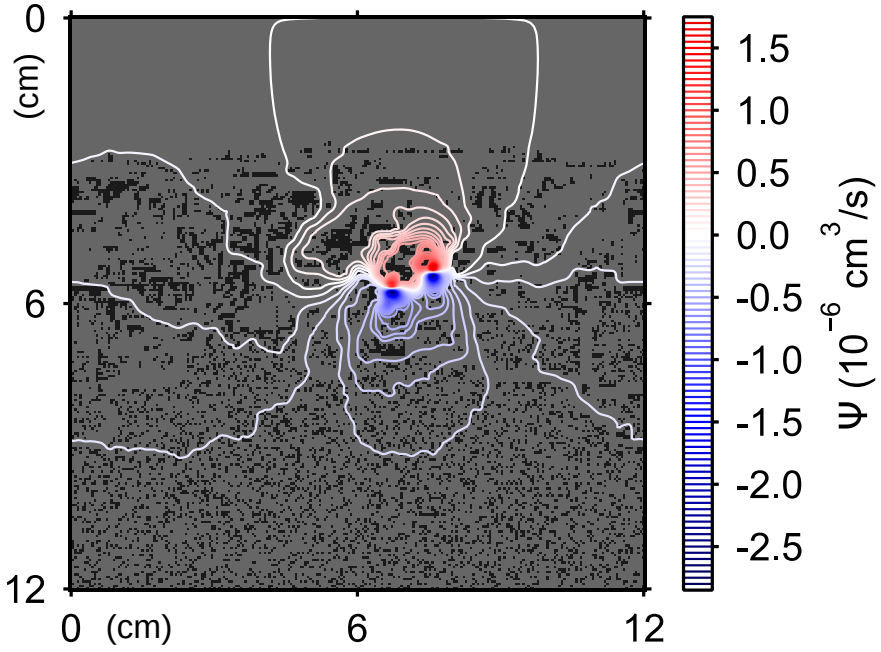

Geosci. Model Dev. Discuss., https://doi.org/10.5194/gmd-2019-62
Manuscript under review for journal Geosci. Model Dev.
Discussion started: 25 April 2019

Geoscientific Model Development Discussions
Open Access
EGU

Figure 4

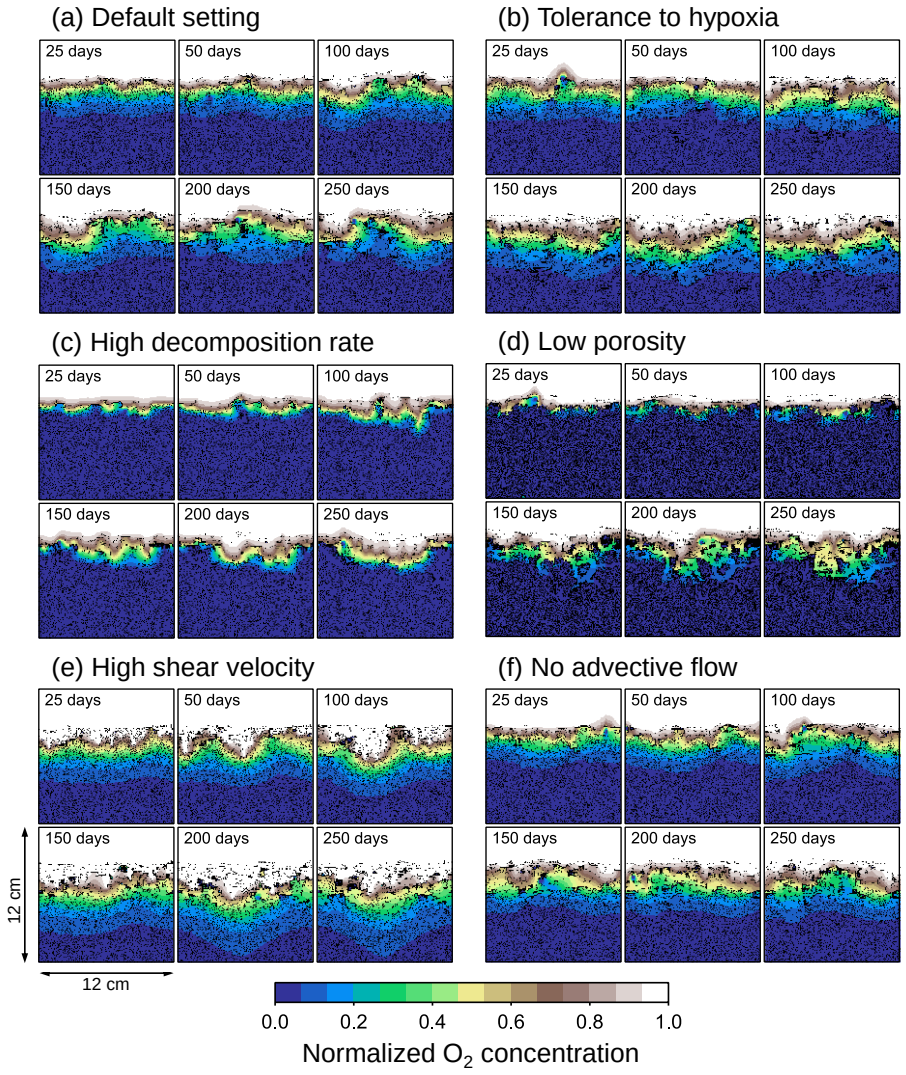

Geosci. Model Dev. Discuss., https://doi.org/10.5194/gmd-2019-62
Manuscript under review for journal Geosci. Model Dev.
Discussion started: 25 April 2019

Figure 5

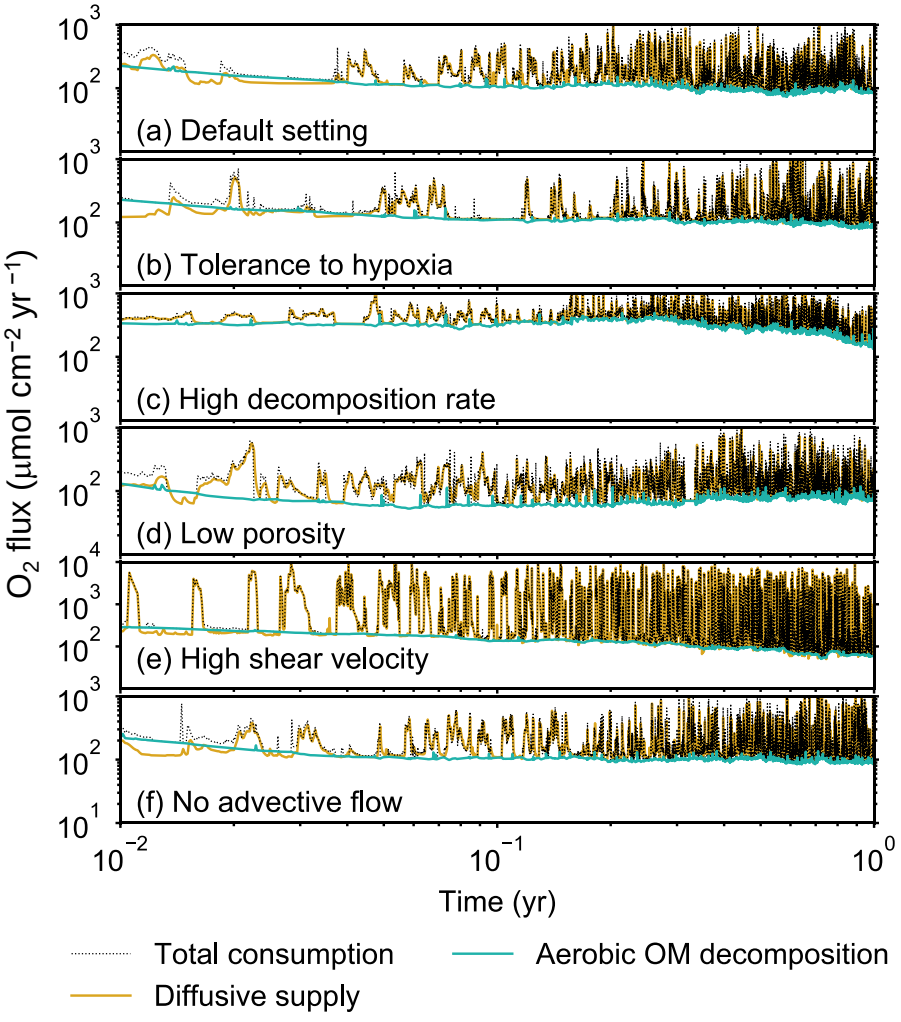

Geosci. Model Dev. Discuss., https://doi.org/10.5194/gmd-2019-62
Manuscript under review for journal Geosci. Model Dev.
Discussion started: 25 April 2019

Geoscientific Model Development Discussions
Open Access
EGU

Figure 6

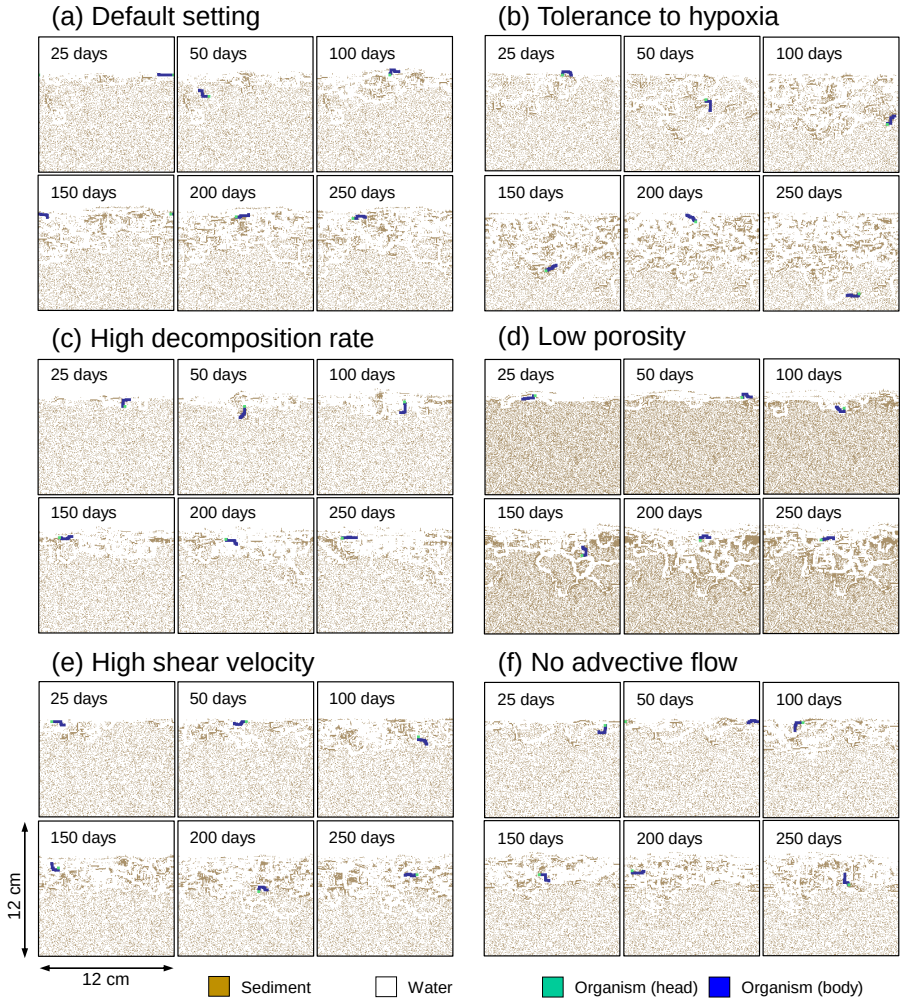

Geosci. Model Dev. Discuss., https://doi.org/10.5194/gmd-2019-62
Manuscript under review for journal Geosci. Model Dev.
Discussion started: 25 April 2019

Geoscientific Model Development Discussions
Open Access
EGU

Figure 7

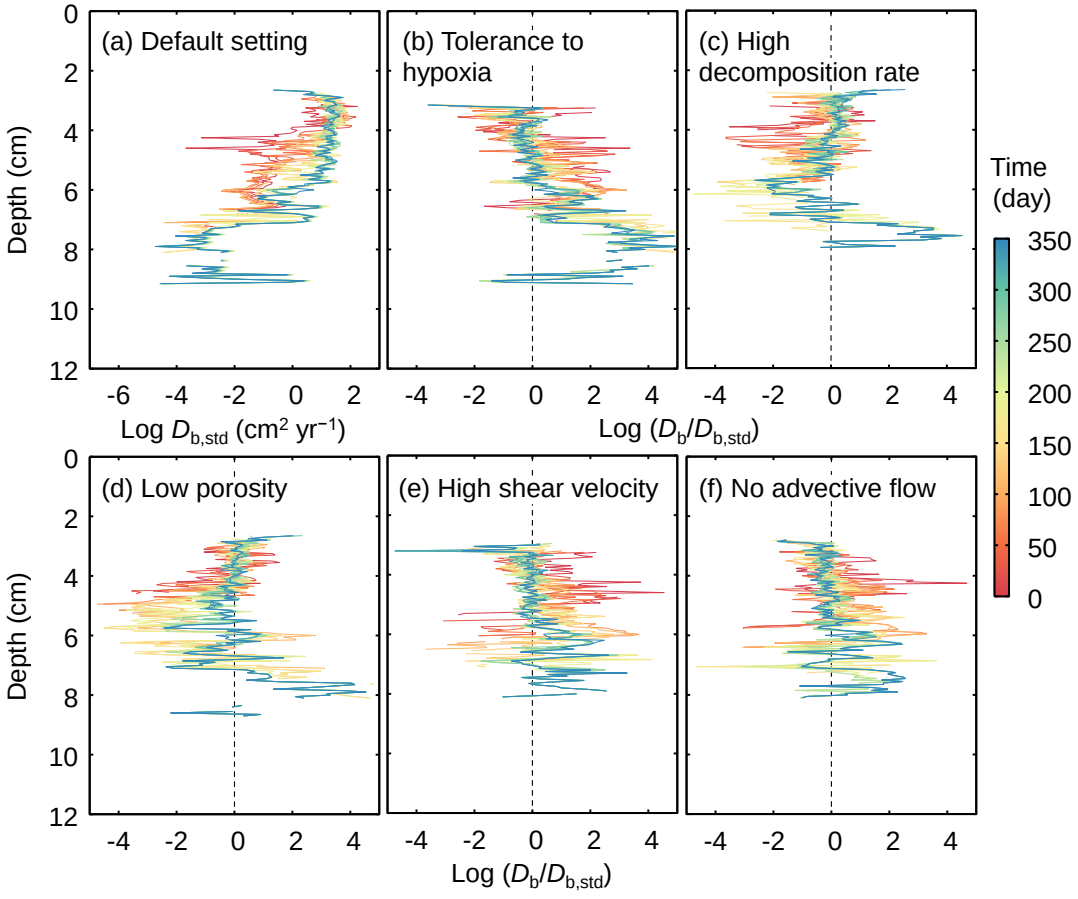

Geosci. Model Dev. Discuss., https://doi.org/10.5194/gmd-2019-62
Manuscript under review for journal Geosci. Model Dev.
Discussion started: 25 April 2019

Geoscientific Model Development Discussions
Open Access
EGU

Figure 8

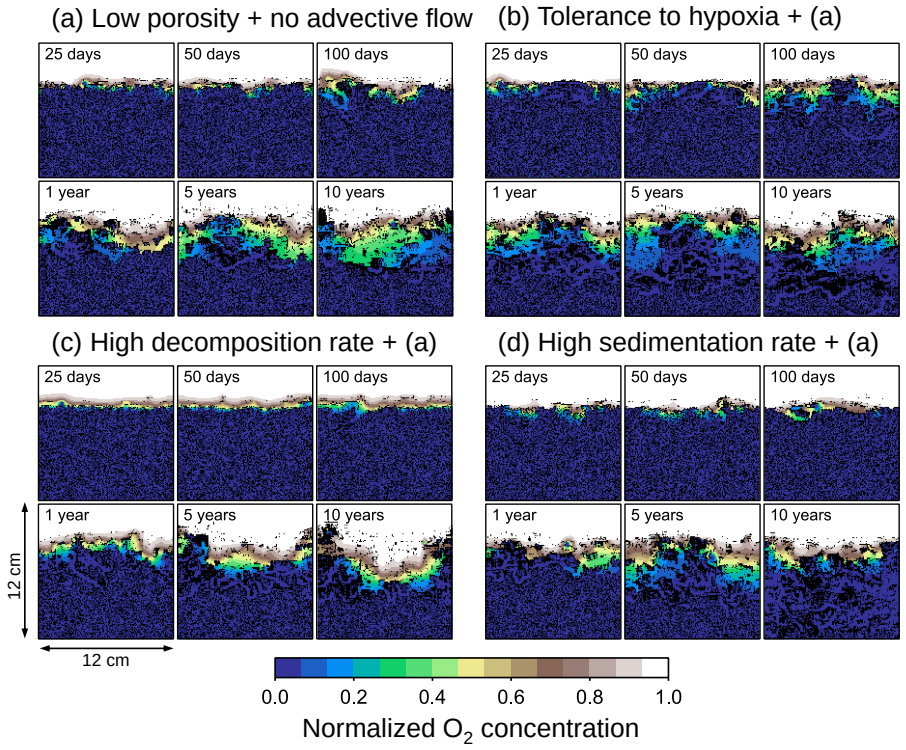

Geosci. Model Dev. Discuss., https://doi.org/10.5194/gmd-2019-62
Manuscript under review for journal Geosci. Model Dev.
Discussion started: 25 April 2019

Geoscientific Model Development Discussions
Open Access
EGU

Figure 9

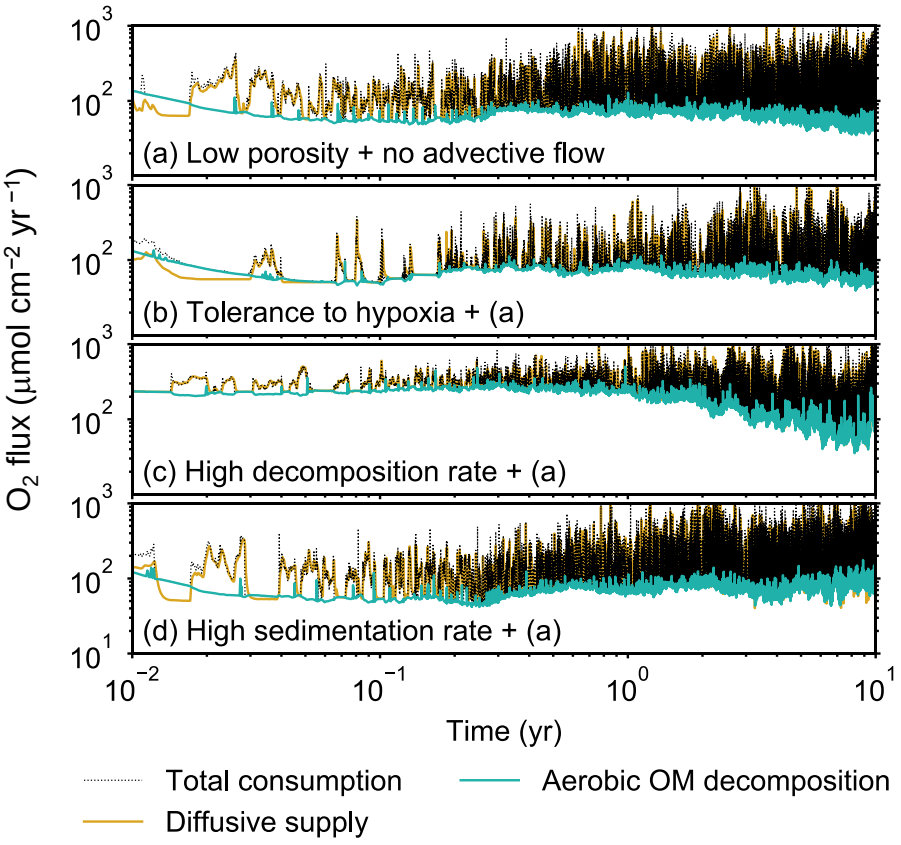

Geosci. Model Dev. Discuss., https://doi.org/10.5194/gmd-2019-62
Manuscript under review for journal Geosci. Model Dev.
Discussion started: 25 April 2019

Figure 10

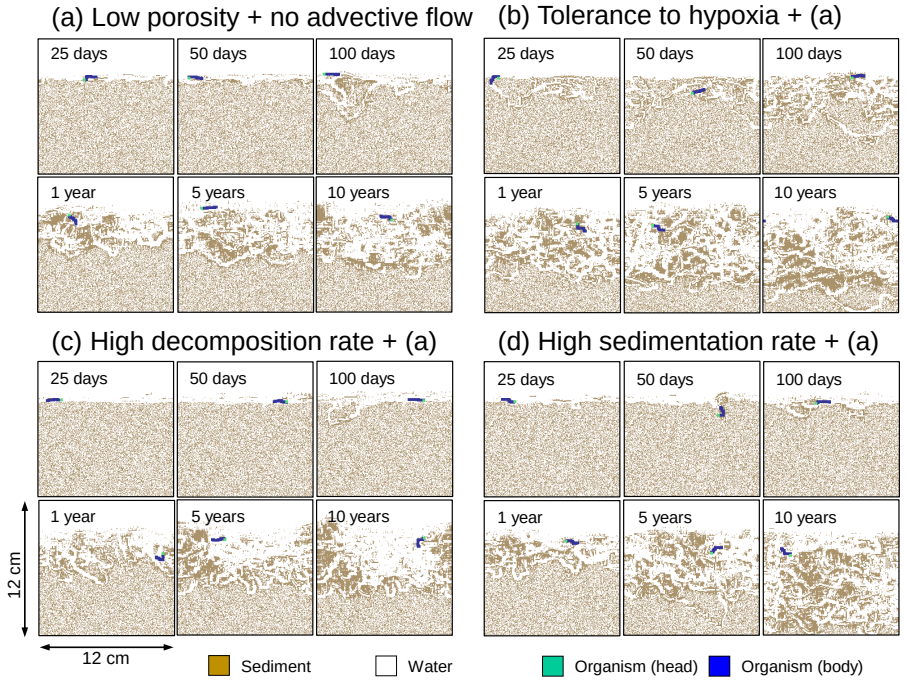

Geosci. Model Dev. Discuss., https://doi.org/10.5194/gmd-2019-62
Manuscript under review for journal Geosci. Model Dev.
Discussion started: 25 April 2019

Figure 11

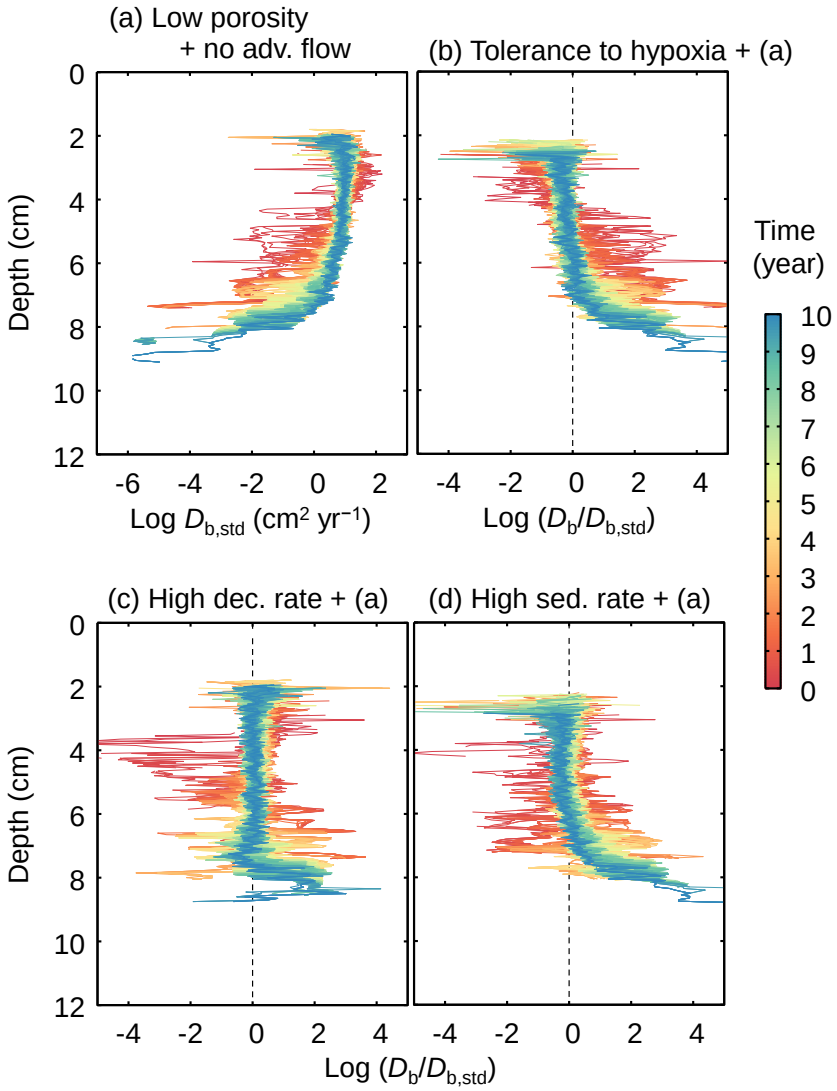

Geosci. Model Dev. Discuss., https://doi.org/10.5194/gmd-2019-62
Manuscript under review for journal Geosci. Model Dev.
Discussion started: 25 April 2019

Figure 12

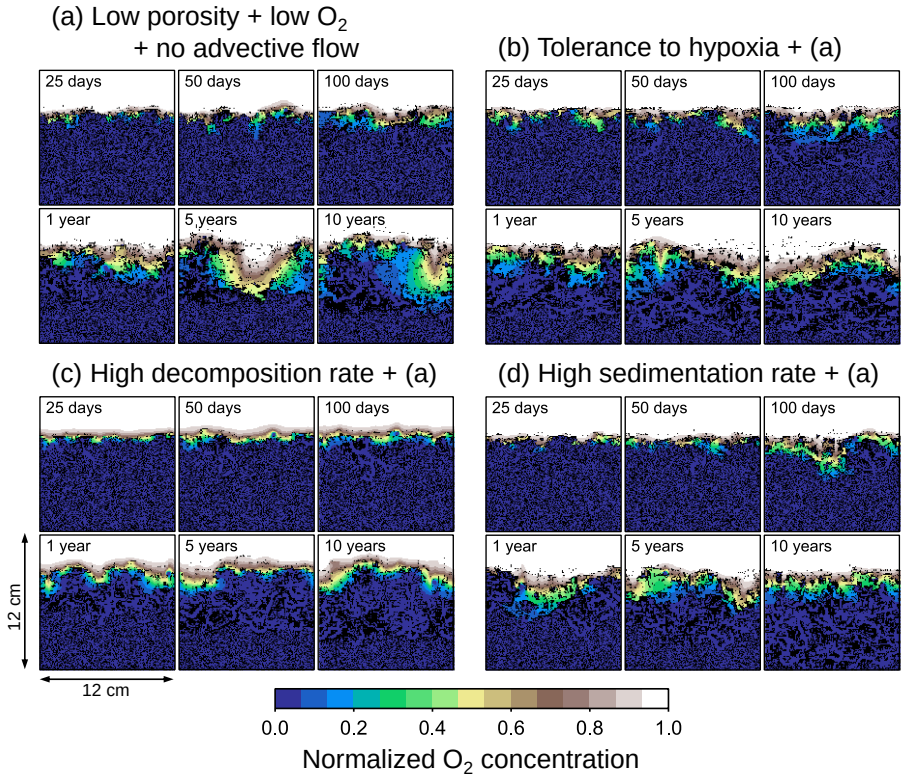

Geosci. Model Dev. Discuss., https://doi.org/10.5194/gmd-2019-62
Manuscript under review for journal Geosci. Model Dev.
Discussion started: 25 April 2019

Geoscientific Model Development Discussions
Open Access
EGU

Figure 13

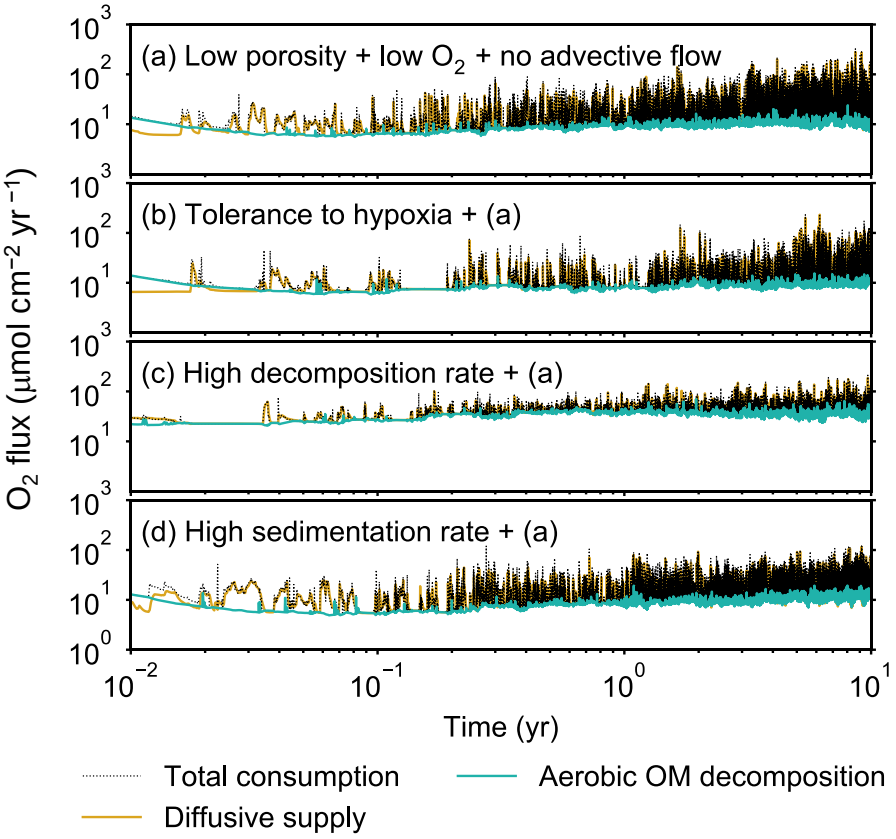

Geosci. Model Dev. Discuss., https://doi.org/10.5194/gmd-2019-62
Manuscript under review for journal Geosci. Model Dev.
Discussion started: 25 April 2019

Geoscientific Model Development Discussions
Open Access
EGU

Figure 14

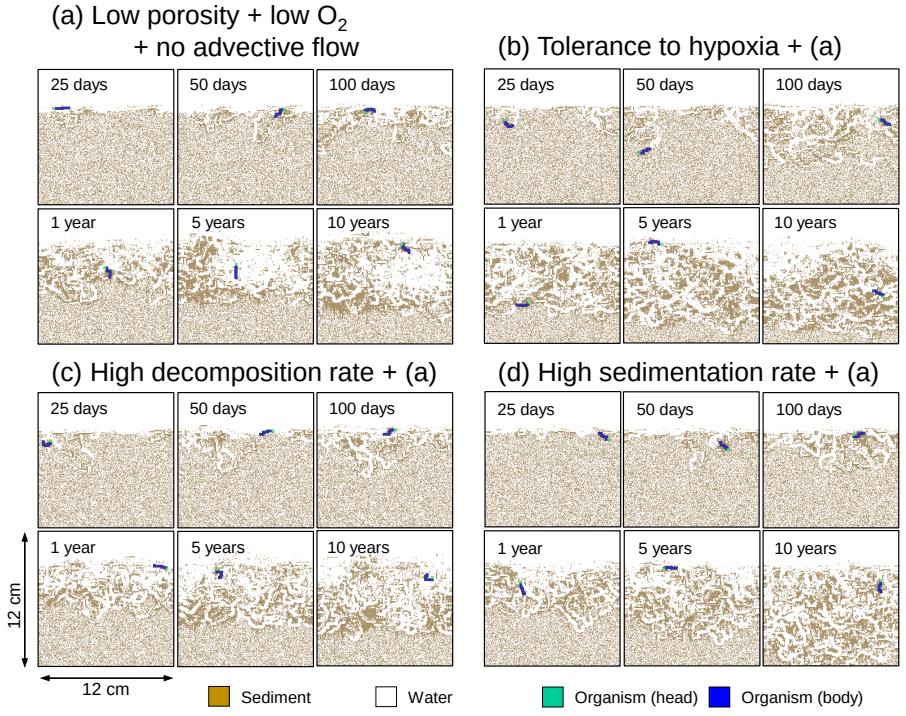

Geosci. Model Dev. Discuss., https://doi.org/10.5194/gmd-2019-62
Manuscript under review for journal Geosci. Model Dev.
Discussion started: 25 April 2019

Figure 15